10

Electromechanics with Thermal and Molecular Diffusion

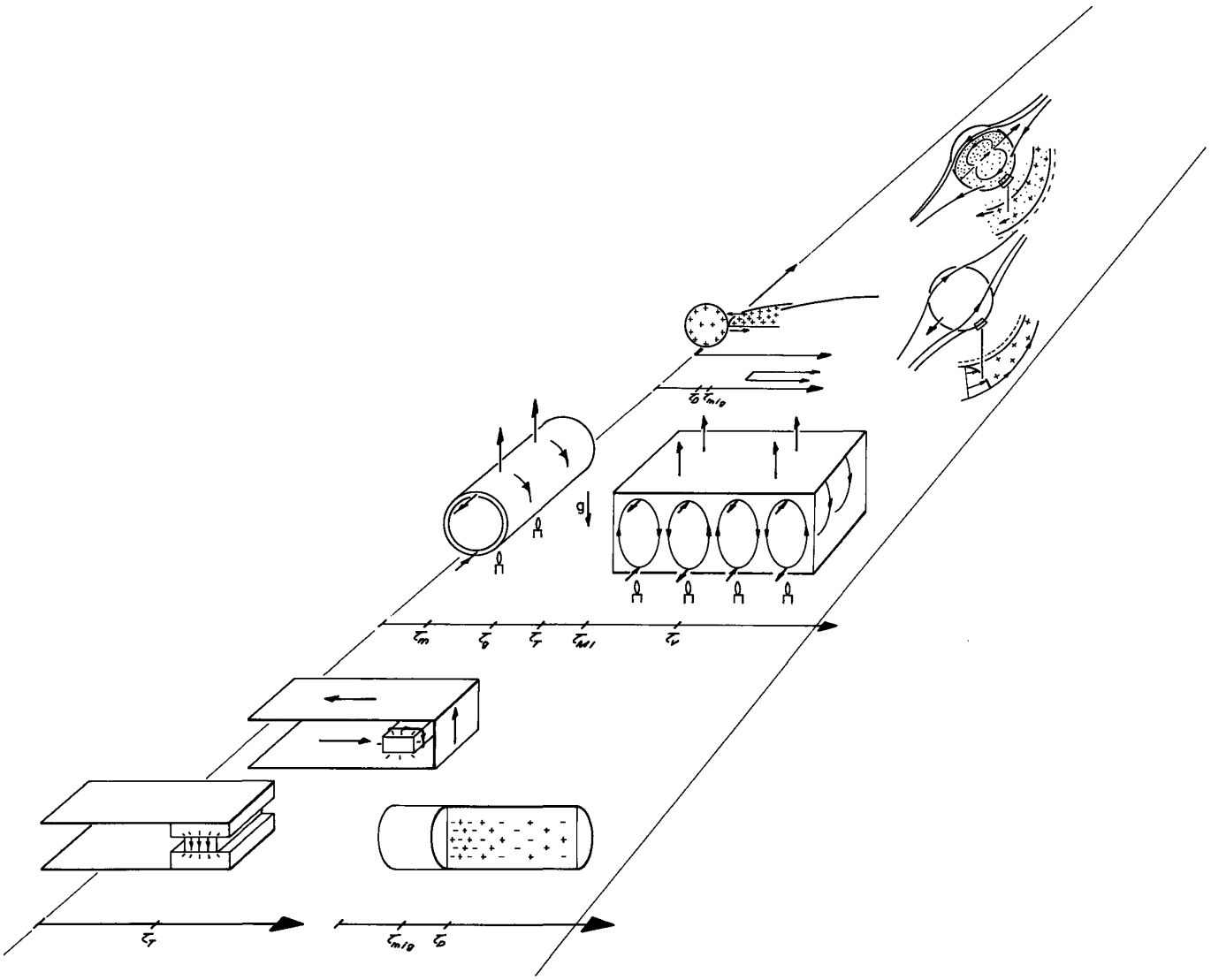

10.1 Introduction

The general three-way coupling between electromagnetic, mechanical and thermal or molecular subsystems might be pictured as in Fig. 10.1.1. Thermal interactions are the subject of the first half of this chapter while the second is concerned with the molecular subsystem.

Diffusion dynamics is familiar from the magnetic diffusion of Chap. 6 and the viscous diffusion of Chap. 7. For both thermal and neutral molecular diffusion processes, Sec. 10.2 builds on this background by identifying the characteristic times, lengths and dimensionless numbers with analogous parameters from these previous dynamical studies. Much of the sinusoidal steady-state and transient dynamics, boundary layer models and transfer relations are equally applicable here.

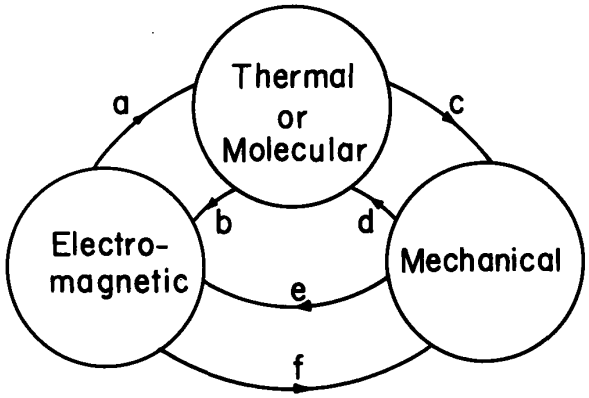

Fig. 10.1.1. Three-way coupling.

Electrical heating and the need for conduction and transport of that heat is often crucial in engineering problems. Section 10.3 is therefore devoted to this one-way coupling in which heat generated electrically in a volume is removed by thermal diffusion, (a) in Fig. 10.1.1. The three-way coupling illustrated in Sec. 10.4 involves an electrical conductivity that is a function of temperature, (b) in Fig. 10.1.1, an electric force created by the resulting property inhomogeneity, (f), and a convection that contributes to the heat transfer, (d).

The rotor model introduced in Sec. 10.5 should incite an awareness of analogies with dynamical phenomena encountered in Chaps. 5 and 6 on circulating fluids, but it should not be forgotten that the diffusion phenomena discussed in many of these sections also occur in solids. The magnetic-field-stabilized Bènard type of instability discussed in Sec. 10.6 is an example of a continuum phenomena that might be modèled by the rotor. This study gives an opportunity to illustrate how the Rayleigh-Taylor types of instability from Chap. 8 are modified if property gradients have their origins in thermal or molecular diffusion.

Because the effect of molecular diffusion of neutral species is similar to that of thermal convection, the sections on molecular diffusion are confined to the diffusion of charged species. Diffusional charging of small macroscopic particles subjected to unipolar ions is the subject of Sec. 10.7. Section 10.8 is aimed at picturing the standoff between diffusion and migration that makes a double layer possible. Based on this simple model, shear-flow electromechanics are modeled in Sec. 10.9 and used to introduce electro-osmosis and streaming potential as electrokinetic phenomena. Another electrokinetic phenomenon, electrophoresis of particles, is taken up in Sec. 10.10. Sections 10.11 and 10.12 introduce electrocapillary phenomena, where the double-layer surface force density from Sec. 3.11 comes into play. Sections 10.7 and 10.8 involve links (a) and (b) in Fig. 10.1.1, while Secs. 10.9, 10.10 and 10.12 involve all links. The sections on molecular diffusion suggest the scale and nature of electromechanical processes found in electrochemical, biological and physiological systems.

10.2 Laws, Relations and Parameters of Convective Diffusion

Thermal Diffusion: The most common thermal conduction constitutive relation between heat flux and temperature is Laplace's law:

$$\vec{f}'_T = -k_T \nabla T \tag{1}$$

where k_T is the coefficient of thermal conductivity. Not only in a perfect gas, but also for many purposes in a liquid, the internal energy is usefully taken as proportional to the temperature. Thus, the energy equation, Eq. 7.23.4, becomes

$$\frac{\partial T}{\partial t} + \vec{v}\cdot\nabla T = K_T \nabla^2 T + \frac{\phi_d}{\rho c_v}; \quad \phi_d \equiv \vec{E}'\cdot\vec{J}'_f + \phi_v - p\nabla\cdot\vec{v} \tag{2}$$

where the thermal diffusivity is defined as $K_T \equiv k_T/\rho c_v$. From left to right, terms in this expression represent the thermal capacity, convection and conduction. The last term is due to electrical and viscous dissipation and power entering the thermal system because of dilatations. Although c_v and k_T are in general functions of temperature, thermally induced variations of other parameters are usually more important and so c_v and k_T have been taken as constant in writing Eq. 2.

Table 10.2.1. Thermal diffusion parameters for representative materials.

Material	Temp. (^oC)	Mass density ρ (kg/m^3)	Specific heat (J/kg^oC)	Thermal conductivity k_T ($watts/m^oK$)	Thermal diffusivity K_T (m^2/s)	Prandtl number $p_T \equiv \frac{\eta}{\rho K_T}$
Liquid			c_p			
Water	10	1.000×10^3	4.19×10^3	0.58	1.38×10^{-7}	9.5
"	30	0.996×10^3	4.12×10^3	0.61	1.46×10^{-7}	5.5
"	70	0.978×10^3	3.96×10^3	0.66	1.61×10^{-7}	2.6
"	100	0.958×10^3	3.82×10^3	0.67	1.66×10^{-7}	1.8
Glycerine	10-70	1.26×10^3	2.5×10^3	0.28	0.89×10^{-7}	1.3×10^4
Carbon tetrachloride	15	1.59×10^3	0.83×10^3	0.11	0.832×10^{-7}	7.3
Mercury	20	13.6×10^3	0.14×10^3	8.0	4.2×10^{-6}	2.7×10^{-2}
CErelow-117	50	8.8×10^3	0.15×10^3	16.5	1.25×10^{-5}	$\sim 5\times10^{-3}$
Gases			c_v			
Air	20	1.20	0.72×10^3	2.54×10^{-2}	2.1×10^{-5}	0.72
"	100	0.95	0.72×10^3	3.17×10^{-2}	3.3×10^{-5}	0.70
Solids			c_p			
Aluminum	25	2.7×10^3	0.90×10^3	240	9.4×10^{-7}	-
Copper	25	8.9×10^3	0.38×10^3	400	11×10^{-7}	-
Vitreous quartz	50	2.2×10^3	0.77×10^3	1.6	9.4×10^{-7}	-

10^{-5} ?

With electrical and viscous heating given, and work done by dilatations negligible (as is usually the case in liquids), Eq. 2 becomes a convective diffusion equation analogous to magnetic diffusion equations in Chap. 6 and viscous diffusion equations in Secs. 7.18-7.20. Instead of the magnetic or viscous diffusion times, the thermal diffusion time

$$\tau_T = \ell^2/K_T \tag{3}$$

characterizes transients having ℓ as a typical length. For processes determined by convection, it is the ratio of this thermal diffusion time to the transport time, ℓ/u, that is relevant. With u a typical fluid velocity, this dimensionless number is defined as the thermal Peclet number,

$$R_T = \ell u/K_T \tag{4}$$

The response to sinusoidal steady-state thermal excitations with angular frequency ω is likely to have a spatial scale that is much shorter than other lengths of interest, in which case the thermal diffusion skin depth

$$\delta_T = \sqrt{\frac{2K_T}{\omega}} \tag{5}$$

is the length over which the thermal inertia of the bulk equilibrates the oscillatory conduction of heat. It is this length that makes $\omega\tau_T = 2$.

Typical thermal parameters are given in Table 10.2.1. In liquids, c_p and c_v are essentially equal. Even at relatively low frequencies the thermal skin depth is perhaps shorter than might be intuitively expected, as illustrated by Fig. 10.2.1.

Molecular Diffusion of Neutral Particles: The analogy between thermal and molecular diffusion is evident from a comparison of the equation for conservation of neutral particles (Eq. 5.2.9 with b = 0, G - R = 0 and $\rho_i \to n$),

$$\frac{\partial n}{\partial t} + \vec{v}\cdot\nabla n = K_D\nabla^2 n \tag{6}$$

to Eq. 2. Transient molecular diffusion, steady diffusion in a steady flow and periodic diffusion are respectively characterized by

$$\tau_D = \ell^2/K_D \qquad \text{molecular diffusion time} \qquad (7)$$

$$R_D = \ell U/K_D \qquad \text{molecular Peclet number} \qquad (8)$$

$$\delta_D = \sqrt{2K_D/\omega} \qquad \text{molecular diffusion skin depth} \qquad (9)$$

Typical parameters are given in Table 10.2.2. The molecular diffusion skin depth is presented as a function of frequency in Fig. 10.2.1, where it can be compared to the thermal skin depth for representative fluids and solids. Simple kinetic models support the observation that, in gases, molecular and thermal diffusion processes have comparable characteristic numbers.[1] Relatively long molecular diffusion times, high molecular Peclet numbers and short skin depths typify liquids on ordinary length scales. In liquids, the molecular diffusion processes occur much more slowly than for thermal diffusion.

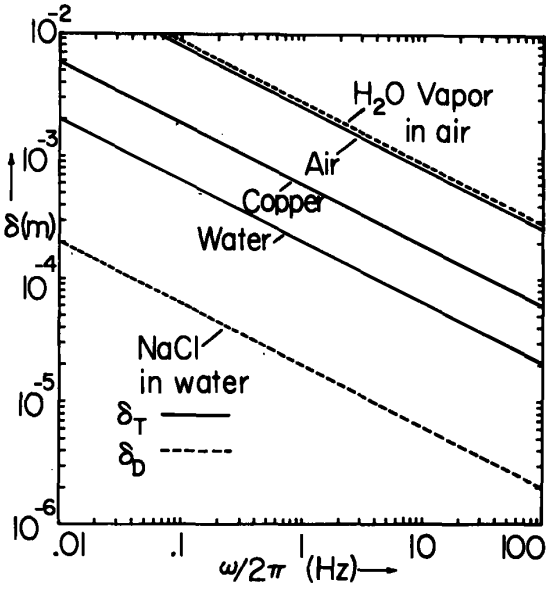

Fig. 10.2.1. Skin depth for sinusoidal steady-state diffusion of heat (solid lines) and molecular diffusion (broken lines) at frequency $f = \omega/2\pi$.

Convection of Properties in the Face of Diffusion: One of the most common ways in which coupling arises between the diffusion subsystem and either the electromagnetic or mechanical subsystem is through the dependence of properties on temperature or concentration. The electrical conductivity is an example. In liquids, it can be a strong function of temperature. If $\sigma = \sigma(T)$, it follows from Eq. 2 that

$$\frac{D\sigma}{Dt} = \frac{\partial\sigma}{\partial T}\frac{DT}{Dt} = \frac{\partial\sigma}{\partial t}\left[K_T\nabla^2 T + \frac{\phi_d}{\rho c_v}\right] \qquad (10)$$

so that, in the absence of diffusion and heat generation, the conductivity is a property carried by the material. That is, the right-hand side of Eq. 10 is zero. Subsequent to the transport of material having an enhanced conductivity into a region of lesser σ, the diffusion tends to return the temperature, and hence the conductivity, to the local value.

In a liquid, the electrical conductivity is linked to the molecular diffusion in a more complicated way. Suppose that an ionizable material is added to a fluid, which in the absence of the added material does not have an appreciable conductivity. Ionization is into bipolar species having charge densities $\rho_\pm$ with the unionized material having the number density, n.

The conservation equations for such a system were written in terms of the net charge density and conductivity in Sec. 5.9, Eqs. 9-11. Written in normalized form, the terms in these equations can be sorted out by establishing an ordering of the intrinsic times relative to times of interest, τ. Typical of relatively conducting, certainly aqueous electrolytes, is the ordering shown in Fig. 10.2.2. Because $\tau/\tau_{th} >> 1$, generation and recombination terms dominate all others in the conservation of neutrals expression, Eq. 5.9.11. It follows that

$$n = \sigma^2 - \frac{(b_+ - b_-)}{b_+ + b_-}\frac{\tau_e}{\tau_{mig}}\sigma\rho_f - \frac{b_+b_-}{(b_+ + b_-)^2}\left(\frac{\tau_e}{\tau_{mig}}\right)^2\rho_f^2 \qquad (11)$$

In the net charge density equation, Eq. 5.9.9, $\tau/\tau_e >> 1$, so that the convective derivative on the left and the last term on the right are negligible compared to the other terms. Hence, that expression becomes

$$\vec{E}\cdot\nabla\sigma + \sigma\rho_f = \frac{\tau_{mig}}{\tau_D}\frac{(K_+ - K_-)(b_+ + b_-)}{K_+b_- + K_-b_+}\nabla^2\sigma \qquad (12)$$

In Eq. 5.9.10, the first term on the right, multiplying τ/τ_{mig}, is expressed using Eq. 12, the second is negligible because $\tau_e/\tau_{mig} << 1$, the third through the sixth cancel by virtue of Eq. 11, while

1. J. O. Hirschfelder, C. F. Curtiss and R. B. Bird, Molecular Theory of Gases and Liquids, John Wiley & Sons, New York, London, 1954, pp. 9-16.

Table 10.2.2. Typical molecular diffusion parameters.[2]

(Prandtl number $p_D \equiv \eta/\rho K_D$).

Material	in	Liquid	Temperature (°C)	Diffusion coefficient K_D (m^2/s)	Molecular Prandtl number $p_D=\tau_D/\tau_v=\eta/\rho K_D$
NaCl		H_2O	18	1.3×10^{-9}	770
			5	0.9×10^{-9}	1700
KNO_3		H_2O	18	1.5×10^{-9}	670
HCl		H_2O	19	2.5×10^{-9}	400
KCl		H_2O	18	1.5×10^{-9}	670
I_2		Ethyl alcohol	18	1.1×10^{-9}	
Material	in	Gas		K_D*	p_D†
O_2		Air		$K_o = 1.78 \times 10^{-5}$	0.8
H_2		N_2		$K_o = 6.74 \times 10^{-5}$	0.2
H_2O		Air		$K_o = 2.20 \times 10^{-5}$	0.7

*For these gases, $K_D = K_o(T/273)^2/p$; T in °K, p in atms.

†Evaluated at 0°C.

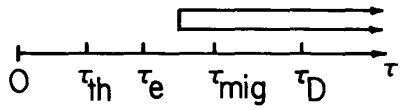

Fig. 10.2.2

Hierarchy of characteristic times for ambipolar diffusion of conductivity.

because $\tau_e \ll \tau_{mig}$, the last term is negligible compared to the next-to-last term. Hence, in dimensional form, the expression becomes

$$\frac{D\sigma}{Dt} = K_a \nabla^2 \sigma; \quad K_a \equiv \frac{K_+ b_- + K_- b_+}{b_+ + b_-} \tag{13}$$

Thus, the conductivity is subject to convective diffusion, but with the ambipolar diffusion coefficient, K_a. Although oppositely charged ions may have different mobilities and diffusion coefficients, the electric field generated by separation of species tends to make the species diffuse together. According to Eq. 12, the net charge can relax essentially instantaneously. Given the distribution of σ from Eq. 13, coupled through $\vec{v}$ to the mechanical subsystem, Eq. 12 can be used to find the distribution of net charge density and hence the force density.

2. For further data and indication of accuracy see E. W. Washburn, International Critical Tables, Vol. 5, McGraw-Hill Book Company, New York, 1929, p. 63.

10.3 Thermal Transfer Relations and an Imposed Dissipation Response

Fully developed flows responding to imposed force densities (Secs. 9.3-9.5) are similar in their description to the sinusoidal steady-state thermal diffusion exemplified in this section. Dissipation densities and material deformation are known, and therefore not influenced by the resulting distribution of temperature and heat flux.

A typical example, shown in Fig. 10.3.1, is an MQS induction system in which a conducting layer having thickness Δ is subject to currents induced by tangential magnetic fields at the upper and lower surfaces:

$$H_y^{\alpha} = \mathrm{Re}\hat{H}_y^{\alpha} e^{j(\omega t - ky)}; \quad H_y^{\beta} = \mathrm{Re}\hat{H}_y^{\beta} e^{j(\omega t - ky)} \tag{1}$$

The layer, which might be a developed model for the conductor in a rotating machine, translates in the y direction with the velocity U. Given the electrical dissipation density $\phi_d = \vec{J}_f \cdot \vec{E}'$, what is the distribution of temperature in the layer? This density has a time-average part that depends only on x and a second harmonic traveling-wave part that depends on (x,y,t). Fortunately, for a given motion, the conduction equation, Eq. 10.2, is linear,

$$\frac{\partial T}{\partial t} + U\frac{\partial T}{\partial y} - K_T \nabla^2 T = \frac{\phi_d}{\rho c_v} \tag{2}$$

so that a transfer relation approach can be taken that combines ideas familiar from Secs. 2.16, 4.5 and 9.3. The system is in the temporal and spatial sinusoidal steady state.

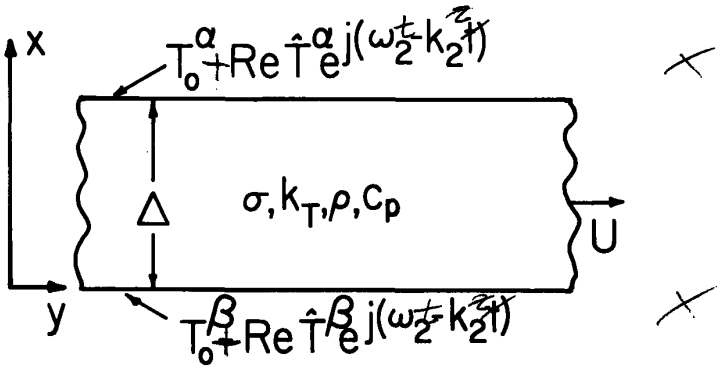

Fig. 10.3.1. Electrical dissipation due to currents induced in moving layer result in steady and second-harmonic temperature response.

Electrical Dissipation Density: The traveling-wave magnetic excitations at the (α,β) surfaces are in general determined by the structure outside the layer. If the layer is bounded by current sheets backed by infinitely permeable material, the amplitudes $(\hat{H}_y^{\alpha}, \hat{H}_y^{\beta})$ are simply $(-\hat{K}_z^{\alpha}, \hat{K}_z^{\beta})$. Regardless of the specific system, magnetic diffusion in the layer is described by the transfer relations (b) of Table 6.5.1. In terms of the resulting amplitudes $(\hat{A}^{\alpha}, \hat{A}^{\beta})$, the distribution of the vector potential follows from Eq. 6.5.6:

$$\hat{A} = \hat{A}^{\alpha}\frac{\sinh \gamma_m x}{\sinh \gamma_m \Delta} - \hat{A}^{\beta}\frac{\sinh \gamma_m (x-\Delta)}{\sinh \gamma_m \Delta}; \quad \gamma_m = \sqrt{k^2 + j\mu\sigma(\omega - kv)} \tag{3}$$

The electrical dissipation follows by evaluating

$$\phi_d = \vec{E}' \cdot \vec{J}_f' = \frac{\vec{J}_f \cdot \vec{J}_f}{\sigma} = \frac{1}{2\sigma}[\hat{J}_z \hat{J}_z^* + \mathrm{Re}\hat{J}_z^2 e^{j(2\omega t - 2ky)}] \tag{4}$$

with the current density related to $\hat{A}$ by Eq. 6.7.5,

$$\hat{J}_z = -\frac{1}{\mu}\left(\frac{d^2 A}{dx^2} - k^2 \hat{A}\right) = -j\sigma(\omega - kU)\hat{A}(x) \tag{5}$$

Thus, the dissipation density is determined, with a steady x-dependent part and a second-harmonic traveling-wave component,

$$\phi_d = \phi_o(x) + \mathrm{Re}\hat{\phi}(x) e^{j(2\omega t - 2ky)} \tag{6}$$

where

$$\phi_o = \frac{1}{2}\sigma(\omega - kU)^2 \hat{A}\hat{A}^*; \quad \hat{\phi} = -\frac{1}{2}\sigma(\omega - kU)^2 \hat{A}^2$$

The temperature response is now the superposition of parts that are respectively due to the steady and

to the second-harmonic drives,

$$T = T_o(x) + \mathrm{Re}\hat{T}(x)e^{j(\omega_2 t - k_2 y)} \tag{7}$$

where $\omega_2 \equiv 2\omega$ and $k_2 \equiv 2k$.

Steady Response: Because the steady dissipation depends only on x and the system extends to infinity in the y directions, Eq. 1 reduces to

$$\frac{d^2T_o}{dx^2} = -\frac{\phi(x)}{k_T} \tag{8}$$

This expression is integrated twice, using as boundary conditions that the steady part of the temperatures at $x = \Delta$ and $x = 0$ are respectively T_o^α and T_o^β:

$$T_o = T_o^\beta + \left[\frac{(T_o^\alpha - T_o^\beta)}{\Delta} + \frac{1}{k_T\Delta}\int_o^\Delta\int_o^{x'} \phi_o(x'')dx''dx'\right]x - \frac{1}{k_T}\int_o^x\int_o^{x'} \phi_o(x'')dx''dx' \tag{9}$$

Associated with this steady part of the response is the heat flux

$$\Gamma_o(x) = -k_T\frac{dT_o}{dx} = -\frac{k_T}{\Delta}(T_o^\alpha - T_o^\beta) + \int_o^x \phi_o(x')dx' - \frac{1}{\Delta}\int_o^\Delta\int_o^{x'} \phi_o(x'')dx''dx' \tag{10}$$

The system external to the layer provides constraints on (T_o^α, T_o^β) and $(\Gamma_o^\alpha, \Gamma_o^\beta)$ which, together with Eq. 10 evaluated at the respective surfaces, specialize these general relations.

Traveling-Wave Response: The response to the traveling wave of dissipation can itself be divided into a homogeneous and particular part. Each takes the complex-amplitude form $\mathrm{Re}\hat{T}\exp j(\omega_2 t - k_2 y)$, and so Eq. 2 requires that

$$\left(\frac{d^2}{dx^2} - \gamma_T^2\right)\begin{bmatrix}\hat{T}_H \\ \hat{T}_P\end{bmatrix} = \begin{bmatrix}0 \\ \frac{-\hat{\phi}}{k_T}\end{bmatrix}; \quad \gamma_T^2 \equiv k^2 + \frac{j(\omega_2 - k_2 U)}{K_T} \tag{11}$$

The homogeneous expression takes the same form, Eq. 2.16.13 with $\gamma \to \gamma_T$, as for the flux-potential relations from Table 2.16.1, so the heat-flux temperature transfer relations can be written by analogy:

$$\begin{bmatrix}\hat{\Gamma}_H^\alpha \\ \hat{\Gamma}_H^\beta\end{bmatrix} = k_T\gamma_T\begin{bmatrix}-\coth\gamma_T\Delta & \frac{1}{\sinh\gamma_T\Delta} \\ \frac{-1}{\sinh\gamma_T\Delta} & \coth\gamma_T\Delta\end{bmatrix}\begin{bmatrix}\hat{T}_H^\alpha \\ \hat{T}_H^\beta\end{bmatrix} \tag{12}$$

The total solution is $\hat{T} = \hat{T}_H + \hat{T}_P$ and it follows that $\hat{T}_H = \hat{T} - T_P$. Substitution of this and the associated heat flux $\hat{\Gamma}_H = \hat{\Gamma} - \Gamma_P$ on the left and right in Eq. 12 results in transfer relations expressing the combined response of the layer to internal and external dissipations:

$$\begin{bmatrix}\hat{\Gamma}^\alpha \\ \hat{\Gamma}^\beta\end{bmatrix} = k_T\gamma_T\begin{bmatrix}-\coth\gamma_T\Delta & \frac{1}{\sinh\gamma_T\Delta} \\ \frac{-1}{\sinh\gamma_T\Delta} & \coth\gamma_T\Delta\end{bmatrix}\begin{bmatrix}\hat{T}^\alpha - \hat{T}_P^\alpha \\ \hat{T}^\beta - \hat{T}_P^\beta\end{bmatrix} + \begin{bmatrix}\hat{\Gamma}_P^\alpha \\ \hat{\Gamma}_P^\beta\end{bmatrix} \tag{13}$$

Any particular solution can be used to evaluate these expressions; but, following the approach used in Sec. 4.5, suppose that both the dissipation density and the particular solution are expressed as a summation of the same modes $\Pi_i(x)$:

$$\hat{\phi} = \sum_{i=0}^{\infty}\hat{\phi}_i\Pi_i(x); \quad \hat{T}_P = \sum_{i=0}^{\infty}\hat{T}_i\Pi_i(x) \tag{14}$$

Then, Eq. 11b shows that these modes satisfy the equation

$$\left(\frac{d^2}{dx^2} + \nu_i^2\right)\Pi_i = 0; \quad \nu_i^2 \equiv \frac{\hat{\phi}_i}{k_T\hat{T}_i} - k_2^2 - \frac{j(\omega_2 - k_2U)}{K_T} \tag{15}$$

Boundary conditions to be satisfied by these modes are a matter of convenience in writing Eq. 13 or expressing Π_i. Here, T_p, and hence Π_i, is taken as zero at the boundaries,

$$\Pi_i = \sin \nu_i x; \quad \nu_i = \frac{i\pi}{\Delta} \tag{16}$$

and it follows from the definition of ν_i, Eq. 15, that

$$\hat{T}_i = \hat{\phi}_i/k_T\left[(\tfrac{i\pi}{\Delta})^2 + k_2^2 + \frac{j(\omega_2 - k_2U)}{k_T}\right] \tag{17}$$

The amplitudes, $\hat{\phi}_i$, are in this case simply Fourier amplitudes evaluated exploiting the orthogonality of the modes, Π_i,

$$\hat{\phi}_i = \frac{2}{\Delta}\int_o^\Delta \hat{\phi}(x)\sin \nu_i x dx \tag{18}$$

Thus, because $T_p = 0$ on the α and β surfaces, the total temperature response to the traveling-wave part of the dissipation is

$$T = \mathrm{Re}\left\{\left[\hat{T}^\alpha \frac{\sinh \gamma_T x}{\sinh \gamma_T \Delta} - \hat{T}^\beta \frac{\sinh \gamma_T(x-\Delta)}{\sinh \gamma_T \Delta}\right] + \sum_{i=1}^{\infty} \hat{T}_i \sin (\tfrac{i\pi}{\Delta} x)\right\} e^{j(\omega_2 t - k_2 y)} \tag{19}$$

In terms of the same temperature amplitudes, $(\hat{T}^\alpha, T^\beta)$, the heat flux at the boundaries follows by evaluating Eq. 13:

$$\begin{bmatrix} \hat{\Gamma}^\alpha \\ \hat{\Gamma}^\beta \end{bmatrix} = k_T\gamma_T \begin{bmatrix} -\coth \gamma_T\Delta & \frac{1}{\sinh \gamma_T\Delta} \\ \frac{-1}{\sinh \gamma_T\Delta} & \coth \gamma_T\Delta \end{bmatrix} \begin{bmatrix} \hat{T}^\alpha \\ \hat{T}^\beta \end{bmatrix} - \sum_{i=1}^{\infty} \frac{(\frac{i\pi}{\Delta})\hat{\phi}_i}{\left[(\frac{i\pi}{\Delta})^2 + k_2^2 + \frac{j(\omega_2 - k_2U)}{K_T}\right]} \begin{bmatrix} (-1)^i \\ 1 \end{bmatrix} \tag{20}$$

These transfer relations between temperatures and heat fluxes at the (α,β) surfaces of the layer, are applicable to the description of different thermal conduction systems in which the layer might be embedded.

In practice, the thermal diffusion skin depth $\delta_T \equiv \sqrt{2k_T/(\omega_2 - k_2U)}$, based on the Doppler frequency $(\omega_2 - k_2U)$, is likely to be short compared either to the thickness of the layer or to half the wavelength of the magnetic field, $2\pi/k_2$. For example, from the curve for copper in Fig. 10.21, $\delta_T \approx .06$ mm at $\omega/2\pi = 100$ Hz. Thus for the lowest values of i in either Eq. 17 or Eq. 20, it is likely that

$$(\tfrac{i\pi}{\Delta})^2 + k_2^2 << \frac{|\omega_2 - k_2U|}{K_T} \equiv \frac{2}{\delta_T'^2} \tag{21}$$

The Fourier coefficients $\hat{T}_i$ are therefore proportional to $\hat{\phi}_i$ for the lowest terms in the series, and the driven response has essentially the same profile over the layer cross section as does the dissipation density. In this case, the thermal capacity absorbs the heat with a 90^o time delay of the temperature relative to the dissipation density. There is insufficient time for the heat to diffuse appreciably. Also note that in this short thermal skin-depth limit these lowest order terms are proportional to $\delta_T'^2$, and so the thermal inertia represented by the heat capacity tends to suppress the oscillatory part of the temperature response.

10.4 Thermally Induced Pumping and Electrical Augmentation of Heat Transfer

By means of a simple one-dimensional flow, illustrated in this section is the three-way interaction between electric, kinetic and thermal subsystems. The flow is essentially incompressible. Shown in Fig. 10.4.1 is a section from a duct for fluid flowing in the y direction. Grids in the planes $y = 0$ and $y = \ell$ constrain the fluid temperatures in these planes to be T_a and T_b, respectively. Typical of many semi-insulators (such as doped hydrocarbons, plasticizers and even chocolate), this liquid has an electrical conductivity that is a function of temperature. For this example,

$$\sigma = \sigma_a[1 + \alpha_T(T - T_a)] \tag{1}$$

where σ and α_T are constant material properties.

With the application of a potential difference, V, between the grids, there is a current density J_o that flows in the y direction between the grids. Continuity requires that J_o be independent of y, and hence that the electric field between the grids be nonuniform. The charge density attending this nonuniformity conspires with the electric field itself to give an electric force density tending to pump the liquid. However, fluid motion implies the convection of heat and a field induced contribution to the temperature distribution and hence to the heat transferred between the grids.

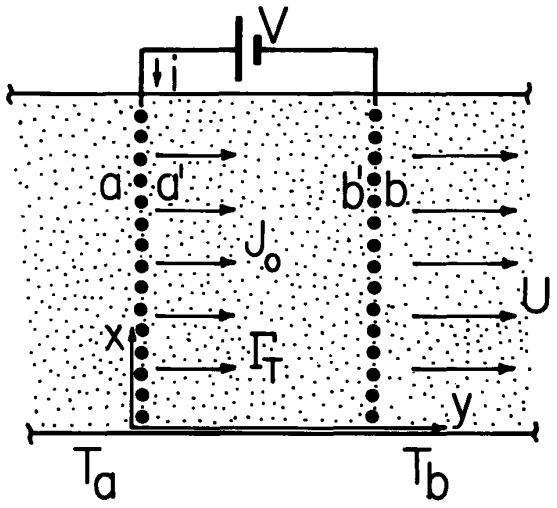

Fig. 10.4.1. Configuration for electrothermally induced pumping and electrically augmented heat transfer.

The width of the channel is large compared to ℓ. Hence, the velocity profile is uniform with respect to the transverse direction. Viscous effects are confined to the flow through the grids and reflected in a pressure drop through each of the grids. Because the flow is one-dimensional and essentially incompressible, $\vec{v} = U\vec{i}_y$. In terms of this velocity and the locations indicated in Fig. 10.4.1, the pressure drops through the grids are taken as

$$p_a - p_{a'} = \frac{c\eta U}{d}; \quad p_{b'} - p_b = \frac{c\eta U}{d} \tag{2}$$

where the dimensionless coefficient c is determined by the geometry of the grids. The dependence of the grid pressure drops on the viscosity and velocity is consistent with flow through the grids at a low Reynolds number based on a characteristic dimension, d, of the grid.

Electrical Relations: Consistent with the geometry is an electric field having the form $\vec{E} = E(y)\vec{i}_y$. It is assumed that in this EQS system, the charge relaxation time, τ_e, is short compared to the thermal diffusion time, τ_T, and that the transport time, ℓ/U, is long compared to τ_e but arbitrary relative to τ_T. That $\tau_e << \ell/U$ means that the convection current density, $\rho_f U$, can be ignored compared to the electrical conduction current density, σE. Thus, even with the fluid motion, Ohm's law is simply $\vec{J} = \sigma\vec{E}$ with σ given by Eq. 1. Because $\vec{J}_f = J_o\vec{i}_y$ is independent of y, this makes it possible to specify E(y) in terms of the yet to be determined temperature distribution, T(y):

$$E = J_o\{\sigma_a[1 + \alpha_T(T - T_a)]\}^{-1} \tag{3}$$

With the terminal current, i, taken as the cross-sectional area, A, times J_o, the electrical terminal relation is then given by

$$V = \int_o^\ell E\,dx = \frac{i}{A\sigma_a}\int_o^\ell \frac{dx}{[1 + \alpha_T(T - T_a)]} \tag{4}$$

Mechanical Relations: Only the longitudinal component of the Navier-Stokes equation is relevant, and because the flow is one-dimensional, neither inertial nor viscous force densities make a contribution between the grids. With the electrical force density written as the divergence of the Maxwell stress ($\rho_f E = d(\tfrac{1}{2}\varepsilon E^2)/dy$), the force equation then becomes simply

$$\frac{\partial}{\partial y}\left(p - \frac{1}{2}\varepsilon E^2\right) = 0 \tag{5}$$

The quantity in brackets is independent of y and can be evaluated by letting $p(0) = p_a$, and $E(0) = E(T = T_a)$. Thus, evaluation of p at $y = \ell$ where $p = p_b$, gives

$$p_a' - p_b' = \frac{1}{2}\varepsilon(E_a^2 - E_b^2) \tag{6}$$

By means of Eqs. 2, this expression is expressed in terms of the pressures just outside the grids:

$$p_b - p_a = -\frac{2c\eta U}{d} + \frac{1}{2}\varepsilon\frac{J_o^2}{\sigma_a^2}\{[1 + \alpha_T(T_b - T_a)]^{-2} - 1\} \tag{7}$$

As with the electrical relations, Eqs. 3 and 4, the temperature distribution is required to evaluate this mechanical terminal relation.

Thermal Relations: With the electrical and viscous dissipations taken as negligible compared to thermal inputs from the grids, the energy equation, Eq. 10.2.2, reduces to

$$\rho c_v U\frac{dT}{dy} = k_T\frac{d^2T}{dy^2} \tag{8}$$

With one integration, this expression simply states that the heat flux, Γ_T, is independent of y:

$$\Gamma_T = -k_T\frac{dT}{dy} + \rho c_v UT \tag{9}$$

The temperature distribution is then determined by solving Eq. 9 subject to the condition that $T(0)=T_a$:

$$T = \frac{\ell\Gamma_T}{k_T R_T}(1 - e^{R_T(y/\ell)}) + T_a e^{R_T(y/\ell)} \tag{10}$$

Here, $R_T \equiv \rho c_v U\ell/k_T$ is the thermal Peclet number.

What might be termed the thermal terminal relation is found by evaluating Eq. 10 at $y = \ell$ where $T = T_b$ and solving for the heat flux, now determined by T_a and T_b and the velocity U (represented by R_T):

$$\Gamma_T = \frac{T_b - T_a e^{R_T}}{1 - e^{R_T}}\frac{k_T R_T}{\ell} \tag{11}$$

By way of emphasizing the degree to which convection contributes to the heat flux, the Nusselt number, N_u, is defined as the ratio of Γ_T to what the flux would be at the same temperature difference if only thermal conduction were present:

$$Nu \equiv \frac{\Gamma_T}{k_T(T_a - T_b)/\ell} = \frac{R_T}{1 - e^{R_T}}\left[\frac{\frac{T_b}{T_a} - e^{R_T}}{1 - \frac{T_b}{T_a}}\right] \tag{12}$$

Given terminal constraints on the external pressure difference, $p_b - p_a$, electrical current, $i = J_o A$ and temperatures T_a and T_b, the remaining variables are now known. The distribution of electric field intensity and the voltage are given by Eqs. 3 and 4. The flow velocity, U, follows from Eq. 7, and hence R_T is determined. Finally, the temperature distribution and heat flux (or Nusselt number) are given by Eqs. 10-12.

Illustrated in Fig. 10.4.2 is N_u as a function of R_T for the case where $T_a > T_b$. From Eq. 7, note that if the flow were re-entrant so that $p_a = p_b$, the fluid velocity and hence R_T would be proportional to J_o^2. Typical distributions of the temperature are shown in the insets to Fig. 10.4.2. Illustrated is the tendency of the convection to skew the temperature profile in the streamwise direction from the linear profile for conduction alone.

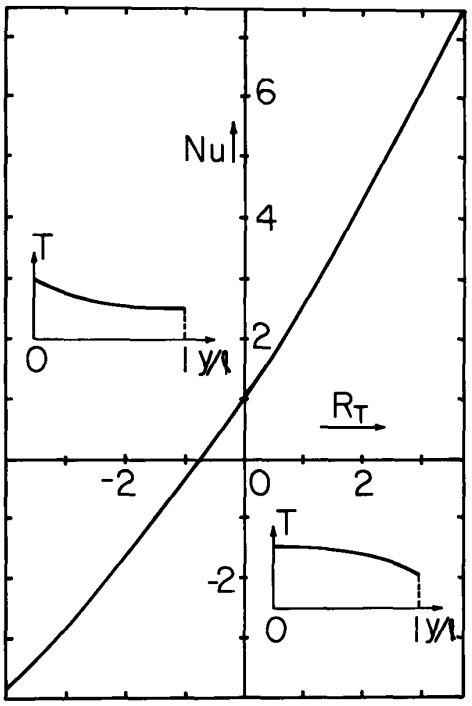

Fig. 10.4.2

Nusselt number as a function of thermal Peclet number for $T_b/T_a = 0.5$. Inserts show temperature distributions typical of positive ($R_T = 4$) and negative ($R_T = -4$) flows.

10.5. Rotor Model for Natural Convection in a Magnetic Field

When heated, most fluids decrease in mass density. In a gravitational field, the result is a tendency for hot fluid to rise and be replaced by falling cold fluid. Heating and cooling systems exploit the transport of heat through the agent of this "natural" convection.

The electrothermal pumping illustrated in Sec. 10.4 is an electromechanical analogue of this process. Gravity is replaced by the electric field and the role of the temperature-dependent mass density taken by the electrical conductivity.

The model developed in this section can be applied to understanding such aspects of thermally induced convection as the instability that starts the convection with the thermally stratified system satisfying conditions for a static equilibrium.

Thermally induced circulations are often undesirable. An example is in the growth of crystals, where convection is a source of imperfections in the product. Especially in liquid metals, it is possible to damp these circulations by applying a magnetic field. Such damping is included in the model.

In Sec. 10.6, the incipience of the instability and its magnetic stabilization are considered again in terms of the more general fluid mechanics, but for small-amplitude circulations. The model developed here retains nonlinear dynamical effects and is similar to models that have proved useful in gaining insights into magnetohydrodynamic circulations of the earth's core.[1]

The cylindrical rotor, shown in Fig. 10.5.1, is both a thermal and an electrical conductor, such as a metal. It is free to rotate with angular velocity Ω. Surrounding the rotor is a jacket, the exterior of which is constrained in temperature to $T_{ext}(\theta)$. Specifically, representing heating from below and cooling from above would be the exterior temperature distribution

$$T_{ext} = T_E - T_e \sin\theta \qquad (1)$$

if T_E were positive.

Heat transferred across the thickness, d, of the layer to the shell has alternative mechanisms for reaching the top of the cylinder and being transferred back across the layer to the exterior. Along the shell periphery, the heat can be thermally conducted, or if the shell turns out to be moving,

1. W. V. R. Malkus, "Non-periodic Convection at High and Low Prandtl Number," Mem. Soc. Roy. Sci. Liège 4 [6], 125-128 (1972).

it can be convected. For conduction alone, the heat flux is symmetric and so also is the temperature distribution. Thus, if there is no motion, thermally induced changes in mass density on the right are the same as to the left, and the effect of gravity gives rise to no net torque. But, if there is motion, conduction of heat is augmented on one side but inhibited on the other, and there is a skewing of the temperature distribution. The result is an expansion of the material on one side that exceeds that on the other, and a net gravitational torque that tends to further encourage the motion. This tendency toward instability that depends on the rate of rotation is countered by two other rate processes. One results in viscous drag from the fluid surrounding the cylinder, modeled here by the thin layer of fluid. As an additional damping mechanism, a magnetic field $\vec{H} = H_o\vec{i}_y$ is imposed. Thus, in response to the motion, z-directed currents are induced in the cylinder in the neighborhoods of the north and the south poles, and these conspire with H_o to produce a rate-dependent damping torque on the rotor.

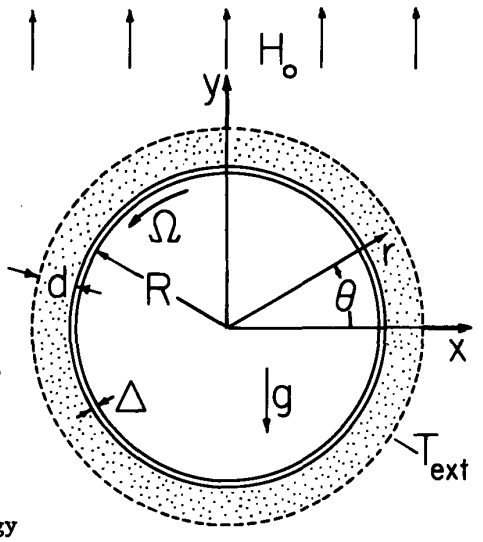

Fig. 10.5.1. Cross section of rotor used to model thermally induced convection.

Heat Balance for a Thin Rotating Shell: An incremental section of the shell, shown in Fig. 10.5.2, is described by the energy equation in integral form, Eq. 7.23.3. Consistent with the materials being only weakly compressible is the neglect of $p\nabla\cdot\vec{v}$. The objective here is a quasi-one-dimensional model playing a heat-transfer role that is analogous to that of the shell models introduced in Sec. 6.3 for magnetic diffusion.

The rate of increase of the thermal energy stored in the section of shell is accounted for by the net convection and conduction of heat into the section plus the volume dissipation,

$$\rho c_v[R(\Delta\theta)\Delta]\frac{\partial T}{\partial t} = -\rho c_v \Delta\Omega R[T(\theta+\Delta\theta) - T(\theta)]$$

$$+ k_T\Delta[\frac{1}{R}\frac{\partial T}{\partial\theta}(\theta+\Delta\theta) - \frac{1}{R}\frac{\partial T}{\partial\theta}(\theta)] - R(\Delta\theta)[\![\Gamma_r]\!] + \phi_d R(\Delta\theta)\Delta \qquad (2)$$

Divided by $\Delta\theta$ and in the limit $\Delta\theta \to 0$, Eq. 2 becomes

$$(\frac{\partial}{\partial t} + \Omega\frac{\partial}{\partial\theta})T = \frac{k_T}{\rho c_v R^2}\frac{\partial^2 T}{\partial\theta^2} - \frac{1}{\Delta\rho c_v}[\![\Gamma_r]\!] + \frac{\phi_d}{\rho c_v} \qquad (3)$$

In the following, it is assumed that the volume dissipation, ϕ_d, associated for example with ohmic heating, is negligible compared to heating from the exterior.

In Eq. 3, the angular velocity (like the temperature) is a dependent variable. The expression is nonlinear. Because the shell can only suffer rigid-body rotation, it is appropriate to reduce the thermal aspects of the problem to "lumped-parameter" terms as well. If the thermal excitation were more complicated than Eq. 1, it would be necessary to represent the temperature distribution in terms of a Fourier series. But for the given single harmonic external temperature distribution, only the first harmonic in the series is required:

$$T = T_o(t) + T_x\cos\theta + T_y\sin\theta \qquad (4)$$

The components (T_x, T_y) represent the components of a "thermal axis" for the cylinder.

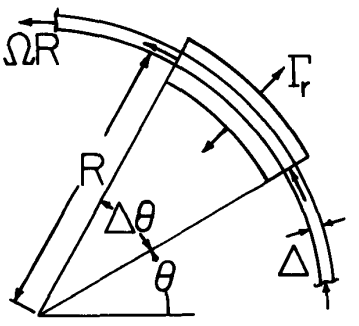

Fig. 10.5.2. Incremental section of thermally conducting moving shell.

Heat flux through the jacket is represented in terms of a surface coefficient of heat transfer, h, so that $\Gamma_r = h(T - T_{ext})$. For pure conduction through a fluid layer having thermal conductivity, k_{Tf}, and thickness d, $h = k_{Tf}/d$.

Substitution of Eq. 4 into Eq. 3 results in terms that are independent of θ and that multiply $\cos\theta$ and $\sin\theta$, respectively. The equation is satisfied by making each of these groups vanish. Hence the three expressions

$$\frac{dT_o}{dt} = -\frac{h}{\Delta\rho c_v}(T_o - T_E) \tag{5}$$

$$\frac{dT_x}{dt} = -\Omega T_y - \frac{k_T}{\rho c_v R^2} T_x - \frac{h}{\Delta\rho c_v} T_x \tag{6}$$

$$\frac{dT_y}{dt} = \Omega T_x - \frac{k_T}{\rho c_v R^2} T_y - \frac{h}{\Delta\rho c_v} T_y - \frac{hT_e}{\Delta\rho c_v} \tag{7}$$

Because T_o only appears in Eq. 5, that expression serves to determine the mean temperature distribution. In the remaining equations, the dependent variables are (T_x, T_y, Ω). Thus, a mechanical (torque) equation for the rotor will complete the description.

Magnetic Torque: Within the electrically conducting shell, Ohm's law (Eq. 6.2.2) requires that the z-directed current density be

$$J_z = \sigma(E_z + \mu_o H_o \Omega R \sin\theta) \tag{8}$$

Here, the magnetic field intensity due to the current in the rotor is ignored. The ends of the cylindrical shell are pictured as being shorted electrically by perfect conductors. Because the electric field in this imposed field approximation is irrotational, and there is no magnetization contribution to Faraday's law, the shorts require that $E_z = 0$ in Eq. 8. Thus, the magnetic torque per unit length in the z direction is

$$\tau_{zm} = -\Delta \int_o^{2\pi} (\vec{J} \times \mu_o H_o \vec{i}_y) R \sin\theta (Rd\theta) = -\Delta R^3 \mu_o^2 H_o^2 \sigma\Omega \int_o^{2\pi} \sin^2\theta = -\Delta R^3 \pi\sigma\mu_o^2 H_o^2 \Omega \tag{9}$$

Consistent with the low magnetic Reynolds number approximation used is a torque proportional to speed that tends to retard the rotation.

Buoyancy Torque: Typically, an increase in temperature results in a decrease in density, although there are exceptions. For small excursions in temperature the surface mass density (kg/m^2) is taken as

$$\sigma_m = \sigma_M[1 - \alpha(T - T_E)] \tag{10}$$

where α is typically positive. Of course, associated with an increase in surface mass density is a local extension of the shell. The resulting effect on the radius tends to be cancelled by contractions elsewhere, but in any case will be neglected. Thus, the net gravitational torque per unit length on the shell is

$$\tau_{zg} = -g \int_o^{2\pi} \sigma_M[1 - \alpha(T - T_E)] R \cos\theta \, Rd\theta \tag{11}$$

With the use of Eq. 4, this integral reduces to

$$\tau_{zg} = \pi g \sigma_M \alpha R^2 T_x \tag{12}$$

A positive T_x means the shell is hotter on the right than on the left, and for positive α, material should tend to rise on the right and fall on the left. As expressed, this buoyancy torque is indeed positive under such circumstances.

Viscous Torque: The fluid in the jacket surrounding the shell is presumed thin enough that its inertia is negligible compared to that of the shell. Also, viscous diffusion is complete in times of interest. Then, the flow can be pictured as plane Couette with a shear stress $-\eta\Omega R/d$. Thus, the viscous torque is

$$\tau_{zv} = -\frac{2\pi\eta R^3}{d}\Omega \tag{13}$$

Torque Equation: The shell has essentially a moment of inertia per unit length $2\pi R^3\sigma_M$. (Small changes due to the expansion are ignored.) Thus, the torques from Eqs. 9, 12 and 13 are set equal to the inertial torque:

$$2\pi R^3\sigma_M \frac{d\Omega}{dt} = -\Delta R^3\pi\sigma\mu_o^2H_o^2\Omega + \pi g\sigma_M\Delta R^2T_x - \frac{2\pi\eta R^3}{d}\Omega \qquad (14)$$

Along with Eqs. 6 and 7, this expression provides a relationship between T_x, T_y, and Ω.

Dimensionless Numbers and Characteristic Times: Normalization of the three equations of motion so that

$$T_x = \underline{T}_x/T_e,\ T_y = \underline{T}_y/T_e,\ t = \underline{t}\tau_T,\ \Omega = \underline{\Omega}/\tau_T \qquad (15)$$

identifies characteristic times:

$$\tau_T \equiv \frac{\rho c_v R^2}{k_T};\quad \tau_t \equiv \frac{\Delta\rho c_v}{h};\quad \tau_g^2 = \frac{R\sigma_M}{g(\sigma_M\alpha T_e)};\quad \tau_m = \mu\Delta R\sigma;\quad \tau_v = \frac{d\sigma_M}{\eta};\quad \tau_{MI}^2 = \frac{R\sigma_M}{\mu_o H_o^2}$$

and dimensionless numbers

$$R_{av} \equiv \frac{Rdg\sigma_M\alpha T_e\rho c_v}{2\eta k_T} = \frac{\tau_v\tau_T}{2\tau_g^2};\quad R_{am} \equiv \frac{Rg\sigma_M\alpha T_e\rho c_v}{\Delta\sigma\mu_o^2H_o^2k_T} = \frac{\tau_{MI}^2\tau_T}{\tau_m\tau_g^2}$$

and leaves Eqs. 6,7 and 14 in the form

$$\frac{dT_x}{dt} = -\Omega T_y - T_x(1 + f) \qquad (16)$$

$$\frac{dT_y}{dt} = \Omega T_x - T_y(1 + f) - f \qquad (17)$$

$$\frac{1}{p_T}\frac{d\Omega}{dt} = -\Omega + R_a T_x \qquad (18)$$

where $\tau_T/\tau_t \equiv f$. Thus, only three dimensionless numbers specify the physical situation, f,

$$R_a \equiv [R_{av}^{-1} + R_{am}^{-1}]^{-1} \text{ and } p_T \equiv \left(\frac{\tau_T}{\tau_v} + \frac{1}{2}\frac{\tau_m}{\tau_{MI}^2}\tau_T\right) \qquad (19)$$

The thermal diffusion and relaxation times τ_T and τ_t, respectively, represent the dynamics of heat conduction in the azimuthal direction and radially through the jacket, in the face of the shell's thermal inertia. The period of a gravitational pendulum having differential surface mass density $\sigma_M\alpha T_e$ and total surface mass density σ_M is familiar from the gravity waves described in Sec. 8.9. The thin-shell magnetic diffusion time, τ_m, is the time for circulating currents to decay (Sec. 6.10), while τ_v is a viscous diffusion time based on the fluid viscosity but the mass density of the shell (Sec. 7.18).

The Rayleigh number, R_a, is large if the time for gravitational acceleration is short (τ_g is small) compared to the geometric mean of the time for viscous slowing of the shell, τ_v, and the time for the shell temperature to return to a uniform distribution, τ_T. Put another way, τ_g^2/τ_v is a gravity-viscous time representing the competition of gravitational and viscous forces.[6] The Rayleigh number is then the ratio of the thermal diffusion time to this gravity-viscous time.

The magnetic Rayleigh number, R_{am}, is large if τ_g is short compared to the geometric mean of τ_T and τ_{MI}^2/τ_m, where the latter is the time required for the magnetic damping to slow the shell despite its inertia.

In the absence of the magnetic field, p_T plays the role of a thermal Prandtl number, the ratio of the thermal to the viscous diffusion time. With negligible viscosity but a magnetic field, the number becomes what might be termed a thermal-magnetic Prandtl number, where the viscous diffusion time is replaced by the time τ_{MI}^2/τ_m.

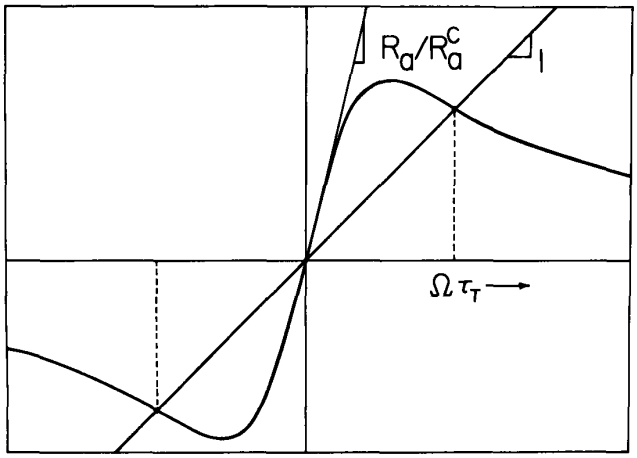

Fig. 10.5.3. Graphical solution of Eq. 21.

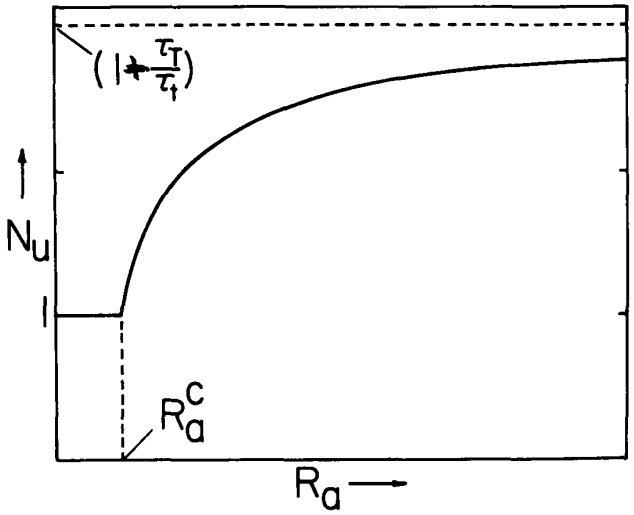

Fig. 10.5.4. Vertical heat flux normalized to flux in absence of rotation as a function of R_a.

Onset and Steady Convection: The similarity between the thermal rotor model and the model for electroconvection developed in Sec. 5.14 (see Prob. 5.14.2) suggests looking for a stationary state. In Eqs. 16-18, the time derivatives are taken as zero and from the first two equations it follows that

$$T_x = \frac{-\Omega T_y}{(1+f)} = \frac{f\Omega}{(1+f)^2+\Omega^2} \tag{20}$$

Hence, the torque equation is expressed in terms of the angular velocity:

$$\Omega = \frac{R_a f\Omega}{(1+f)^2+\Omega^2} \tag{21}$$

The graphical solution of this expression, pictured in Fig. 10.5.3, is familiar from the electric rotor of Sec. 5.14. If R_a is small, the only intersection of the two curves is at the origin and the rotor is stationary. A negative or positive velocity obtains if R_a exceeds R_a^c, where

$$R_a^c = (1+f)^2/f \tag{22}$$

so that the slope of the thermal torque curve at the origin exceeds that of the viscous-magnetic torque curve (which in normalized form is unity). Solution of Eq. 21 gives this velocity and Eqs. 20 give the associated components of the temperature:

$$\Omega = \sqrt{(R_a - R_a^c)f}; \quad T_x = \Omega/R_a; \quad T_y = -(1+f)/R_a \tag{23}$$

These steady conditions are interpreted as the result of an instability having its threshold at $R_a = R_a^c$ and resulting in steady rotation in either direction. As R_a becomes large compared to its critical value, R_a^c, the reciprocal angular velocity is approximated by the product of the gravitational time and the square root of the ratio of the fluid thermal diffusion time to a time representing the combined damping effects of viscosity and magnetic diffusion.

The rotation is reflected in the vertical heat flux. Heat passing into the jacket over the lower half and leaving over the top half is augmented by the motion. From Eq. 5 for the steady motion, it follows that $T_o = T_E$. Using Eqs. 1 and 4, the heat flux is computed from

$$Q_T = \int_o^\pi \Gamma_r R d\theta = \int_o^\pi h(T - T_{ext}) R d\theta = 2hR(T_y + T_e) \tag{24}$$

The Nusselt number, N_u, is now defined as the ratio of this heat flux to what it would be in the absence of rotation (convection),

$$N_u \equiv \frac{Q_T(\Omega)}{Q_T(\Omega=0)} = \frac{1 + T_y(\Omega)}{1 + T_y(0)} \qquad (25)$$

Through Eq. 23, it follows that

$$N_u = \begin{cases} (1 + f)[1 - \dfrac{(1 + f)}{R_a}]; & R_a > R_a^c \\ 1 \qquad\qquad ; & R_a < R_a^c \end{cases} \qquad (26)$$

The Nusselt number is shown as a function of R_a in Fig. 10.5.4. This type of dependence is typical of fluid layers heated from below. At most, the effect of the steady convection is to render the rotor isothermal, but even then conduction through the jacket limits the flux. Hence, the asymptote (1+f) for N_u as $R_a \to \infty$. Raising the magnetic field reduces R_a and hence suppresses the heat flux. Of course, if the magnetic field is large enough to prevent the convection altogether by making $R_a < R_a^c$, then heat transfer is solely due to conduction and $N_u \to 1$.

The dynamical model can be used to study transient behavior. A hint that the predicted phenomena are of great variety is given by considering the stability of the steady rotation just described. Perturbation of the steady rotation shows that oscillatory instability (overstability) can result at high R_a (see Prob. 10.5.1). Because the rotor inertia now comes into play, p_T is therefore a critical parameter.

If heated from the side, the rotor is not in a state of static indeterminancy. It can execute steady rotation in one direction without a threshold. This configuration is also useful for modeling practical natural convection systems. These observations are developed in the problems.

10.6 Hydromagnetic Bénard Type Instability

What is conventionally termed Bénard instability is commonly seen when a layer of cooking oil in the bottom of a pan is heated from below.[1] If heat were applied with perfect uniformity over the horizontal plane, density stratification would result because the lighter fluid is on the bottom. What is seen is cellular convection, as illustrated in Fig. 10.6.1, and it results because, in the gravitational field, the configuration of mass density is unstable, as might be expected from Sec. 8.18. Because material of fixed identity tends to lose its heat to its surroundings, and hence to take on the same mass density, thermal diffusion requires a finite vertical heat flux before the convection is observed.

The rotor of Sec. 10.5 is a finite-amplitude model for this cellular convection. Recognized now are the infinite number of degrees of freedom of the actual fluid, but the continuum model is restricted to perturbations from the static equilibrium.

The layer, shown in Fig. 10.6.2, is horizontal. Driven by a temperature difference $T_b - T_a$, the static layer sustains a uniform vertical heat flux Γ_o. The heat conduction through this static layer is in the steady state, so the temperature distribution is linear and the heat flux independent of x. With DT_s the stationary gradient in temperature, this flux is $\Gamma_o = -k_T DT_s$.

There is no equilibrium magnetic force density, so gravity alone is responsible for the vertical pressure gradient. Conditions for the magnetic Hartmann-type of approximation prevail, in that the magnetic diffusion time, τ_m, is much less than the magneto-inertial time τ_{MI}, while τ_{MI} is much less than the viscous diffusion time, τ_v (see Sec. 9.9). In fact, in this section, viscous effects will be ignored altogether.

The gravitational acceleration of the fluid has its origins in the dependence of the mass density on the temperature. For the relatively small changes in mass density typical of liquids,

$$\rho = \rho_o[1 + \alpha_\rho(T - T_E)] \qquad (1)$$

where ρ_o and α are constants and T_E is the average equilibrium temperature. The coefficient of thermal expansion, α_ρ, is typified in Table 10.6.1.

---

1. S. Chandrasekhar, Hydrodynamic and Hydromagnetic Stability, Clarendon Press, Oxford, 1961, pp.9-75. For effect of magnetic field see pp. 177-186.

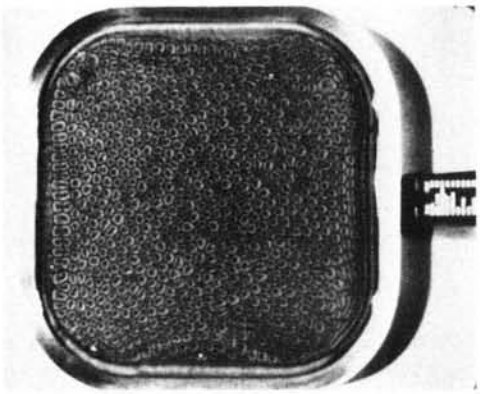

Courtesy of Education Development Center, Inc. Used with permission.

Fig. 10.6.1

Cellular convection subsequent to incipience of thermally induced Bénard instability. A layer of silicone oil is heated from below in a frying pan. (Reference 4, Appendix C).

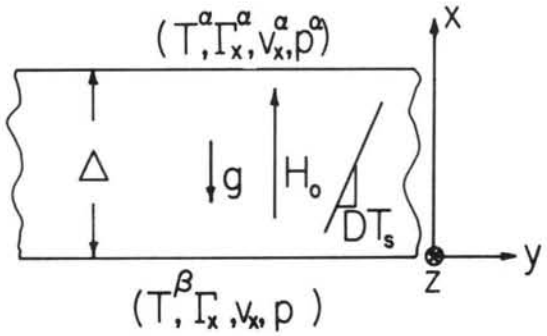

Fig. 10.6.2

Layer of conducting fluid such as liquid metal supporting uniform vertically directed heat flux and magnetic field intensity.

Table 10.6.1. Coefficient of thermal expansion $\alpha_\rho \equiv -(\partial\rho/\partial T)/\rho$ for representative fluids at 200°C

Liquid	Coefficient of thermal expansion α_ρ ($^oC^{-1}$)
Water	-2.1×10^{-4}
Glycerol	-4.7×10^{-4}
Mercury	-1.8×10^{-4}
n-Xylene	-9.9×10^{-4}
Gas (at constant pressure)	
Dry air	-3.4×10^{-3}

For small temperature excursions, mass conservation becomes

$$\nabla\cdot\vec{v} = -\alpha_\rho \frac{DT}{Dt} \tag{2}$$

so the flow is not exactly solenoidal. It is straightforward to include dilatational terms in the force and energy equations, but the additional analytical effort is not justified in the class of flows of interest here. Because α_ρ is small, $\nabla\cdot\vec{v} \simeq 0$. However, it does not follow that the mass density of a given element of fluid remains constant.

The perturbation part of the thermal equation, Eq. 10.2.2 with $\phi_d \simeq 0$, makes evident why the temperature (and hence the mass density) of fluid of fixed identity varies:

$$\frac{\partial T'}{\partial t} + (DT_s)v_x = K_T\nabla^2 T' \tag{3}$$

On the left is the time rate of change of T' for a given element of fluid, and on the right the thermal diffusion that accounts for this rate of change.

The force equation is written neglecting the viscous force density:

$$\rho_o \frac{\partial \vec{v}}{\partial t} + \nabla p = -\rho_o[1 + \alpha_\rho(T_s - T_E)]g\vec{i}_x + \alpha_\rho \rho_o g T' \vec{i}_x + \vec{J} \times \mu_o H_o \vec{i}_x \qquad (4)$$

Consistent with the Hartmann type approximation considered in Sec. 9.9, H_o is imposed both in the force equation and in the constitutive law

$$\vec{J} = \sigma(\vec{E} + \vec{v} \times \mu_o H_o \vec{i}_x) \qquad (5)$$

needed in Eq. 4. Also, because the imposed $\vec{H}$ is constant,

$$\nabla \times \vec{E} \approx 0 \qquad (6)$$

With Eq. 5 substituted into Eq. 4, the pressure is eliminated from the latter by taking the curl. In fact the desired equation for v_x, devoid of $\vec{E}$, is obtained by taking the curl again and exploiting the identity $\nabla \times \nabla \times \vec{v} = \nabla(\nabla \cdot \vec{v}) - \nabla^2 \vec{v}$. Then the x component is simply

$$\rho_o \frac{\mathcal{D}}{\partial t} \nabla^2 v_x = -\alpha_\rho \rho_o g \left(\frac{\partial^2 T'}{\partial y^2} + \frac{\partial^2 T'}{\partial z^2} \right) - \sigma(\mu_o H_o)^2 \frac{\partial^2 v_x}{\partial x^2} \qquad (7)$$

Here, the mass density has been approximated as uniform in the inertial term and $\nabla \cdot \vec{v} \approx 0$. This last approximation is valid provided $\alpha_\rho \ell \Delta T_s \ll 1$, where ℓ is a typical length, perhaps the thickness Δ of the layer. (For a layer of mercury, 1 cm thick, subject to a 100°C temperature difference, this number is 1.8×10^{-2}.) The electric field appears in the other components of the force equation operated on in this fashion, but not in the x component.

In normalized form, Eqs. 3 and 7 become

$$\left[\frac{j\omega}{p_{TM}}(D^2 - k^2) + D^2\right]\hat{v}_x - R_{am} k^2 \hat{T} = 0 \qquad (8)$$

$$\hat{v}_x + [j\omega - (D^2 - k^2)]\hat{T} = 0 \qquad (9)$$

where

$$\omega = \underline{\omega}/(\Delta^2/\kappa_T); \quad \hat{T} = \underline{\hat{T}}\Delta T_s; \quad \hat{\Gamma}_x = \underline{\hat{\Gamma}}_x k_T \Delta T_s$$

$$x = \underline{x}\Delta; \quad \hat{v}_x = \underline{\hat{v}}_x \kappa_T/\Delta; \quad p = \underline{p} \kappa_T^2 \rho_o/\Delta^2$$

$$R_{am} = \frac{\alpha_\rho g \Delta T_s \rho_o \Delta^2}{\kappa_T \sigma (\mu_o H_o)^2} \qquad P_{TM} = \frac{\Delta^2 \sigma (\mu_o H_o)^2}{\kappa_T \rho_o}$$

The variables that complement $(\hat{T}, \hat{v}_x)$ are the thermal flux,

$$\hat{\Gamma}_x = -D\hat{T} \qquad (10)$$

and the pressure, found from the x component of the force equation, Eq. 4, in terms of $(\hat{T}, \hat{v}_x)$:

$$Dp = R_{am} p_{TM} \hat{T} - j\omega \hat{v}_x \qquad (11)$$

The magnetic Rayleigh number and thermal-magnetic Prandtl number are familiar from Sec. 10.5, where they are written as ratios of characteristic times.

Because Eqs. 8 and 9 have constant coefficients, solutions take the form

$$\hat{T} = \sum_{m=1}^{4} \hat{T}_m \exp(\gamma_m x) \qquad (12)$$

$$\hat{v}_x = -\sum_{m=1}^{4} [j\omega - (\gamma_m^2 - k^2)]\hat{T}_m \exp(\gamma_m x) \qquad (13)$$

where the latter follows from Eq. 9. The characteristic equation gotten by substituting into Eqs. 8 and 9 is quadratic in γ^2. Thus, roots take the form $\gamma = \pm\gamma_a$ and $\gamma = \pm\gamma_b$. With $a \equiv -[j\omega - (\gamma_a^2 - k^2)]$ and $b \equiv -[j\omega - (\gamma_b^2 - k^2)]$, the conditions that Eqs. 12 and 13 assume the correct values at the α and β

surfaces are

$$\begin{bmatrix} e^{\gamma_a} & e^{-\gamma_a} & e^{\gamma_b} & e^{-\gamma_b} \\ 1 & 1 & 1 & 1 \\ ae^{\gamma_a} & ae^{-\gamma_a} & be^{\gamma_b} & be^{-\gamma_b} \\ a & a & b & b \end{bmatrix} \begin{bmatrix} \hat{T}_1 \\ \hat{T}_2 \\ \hat{T}_3 \\ \hat{T}_4 \end{bmatrix} = \begin{bmatrix} \hat{T}^\alpha \\ \hat{T}^\beta \\ \hat{v}_x^\alpha \\ \hat{v}_x^\beta \end{bmatrix} \tag{14}$$

The procedure for deducing transfer relations between $[\hat{T}^\alpha,\hat{T}^\beta,\hat{v}_x^\alpha,\hat{v}_x^\beta]$ and $[\hat{\Gamma}_x^\alpha,\hat{\Gamma}_x^\beta,\hat{p}^\alpha,\hat{p}^\beta]$ is now similar to that given in Sec. 7.19. Here attention is confined to the temporal modes and the critical conditions for instability.

Suppose that the boundaries are actually rigid walls, so that $(\vec{v}_x^\alpha,\vec{v}_x^\beta) = 0$, and are constrained to be isothermal, so that $(\hat{T}^\alpha,\hat{T}^\beta) = 0$. Then the determinant of the coefficients in Eq. 14 must vanish. The determinant is easily reduced by subtracting the second and fourth columns from the first and third, respectively. Thus

$$4(b - a)^2 \sinh \gamma_a \sinh \gamma_b = 0 \tag{15}$$

Nontrivial roots to Eq. 15 are either $\gamma_a = jn\pi$ or $\gamma_b = jn\pi$, $n = 1,2,\cdots$. To determine the associated eigenfrequencies $j\omega \equiv s_n$ of the temporal modes, the characteristic equation, found by substituting $\exp(\gamma x)$ into Eqs. 8 and 9,

$$[s_n(\gamma_n^2 - k^2) + p_{TM}\gamma_n^2][s_n - (\gamma_n^2 - k^2)] + p_{TM}R_{am}k^2 = 0 \tag{16}$$

is evaluated with $\gamma_n = jn\pi$. This expression can be solved for s_n to give

$$s_n = \frac{-B \pm \sqrt{B^2 - 4p_{TM}\{(n\pi)^2[(n\pi)^2 + k^2] - R_{am}k^2\}[(n\pi)^2 + k^2]}}{2[(n\pi)^2 + k^2]} \tag{17}$$

where $B \equiv p_{TM}(n\pi)^2 + [(n\pi)^2 + k^2]^2$. Provided that the quantity in {} under the radical is greater than zero, all roots are negative, because then the radical has a magnitude less than B. However, if that term is negative, half of the roots represent growing exponentials. Thus, the critical condition for the onset of cellular convection of each mode, n, at a wavelength $2\pi/k$ is

$$R_{am} = \frac{(n\pi)^2}{k^2}[(n\pi)^2 + k^2] \tag{18}$$

Note that R_{am} is indeed positive for the typical fluid heated from below, because α_ρ is typically negative and DT_s is also negative. In addition to the transverse modal structure represented by n, there is the longitudinal dependence represented by k. According to the model, the n = 1 mode with infinitely short wavelength (infinite k) is the most critical with incipience at

$$R_{am}^c = \pi^2 \tag{19}$$

To have a better approximation as to the critical longitudinal wavelength of the most critical mode, it would be necessary to add further physical processes, such as viscous diffusion, to the model. The way in which viscosity plays the damping role of the magnetic field is illustrated in Sec. 10.5 and Prob. 10.6.3.

In the rotor model, there are two thermal time constants, with a ratio $\tau_T/\tau_t \equiv f$. In the fluid layer, there is no such dimensionless ratio, because azimuthal and radial conditions involve the same spatial scale and the same fluid properties. Hence, the critical Rayleigh number that is equivalent to Eq. 19 is given by Eq. 10.5.22. The steady convection and overstability of that convection predicted using the rotor model give some hint as to the nonlinear phenomena that ensue as R_{am} is raised beyond R_a^c. At first, due to cellular convection, there is an augmentation of the heat transfer, as typified by a Nusselt number that increases with R_a. The steady cellular motion is itself potentially unstable with an ultimate turbulent (nonsteady) state the result. The transition to turbulence should be expected to be a function not only of R_a but also of p_T.

10.7 Unipolar-Ion Diffusion Charging of Macroscopic Particles

Ions encountering the surface of a macroscopic particle tend to become attached. This is especially true in gases, where macroscopic particles are commonly charged in passage through an ion filled region. This is illustrated in Sec. 5.5, where an imposed electric field is responsible for the migration of ions to the surface of the particle. The result is "impact" or "field" charging. The model in Sec. 5.5 neglects the fact that, on a sufficiently small scale, there is also a diffusional contribution to the ion flux. Through diffusion, ions also reach the surface and hence charge the particle. This contribution can exceed that due to impact for sufficiently small particles.

As diffusion charging proceeds, it does so at a decreasing rate because the electric field generated by the charging tends to produce an ion migration that counters the ion diffusion. The determination of this charging rate and hence of the particle charge gives the opportunity to discuss some general features of the diffusion of a single charged species while obtaining a useful result.

The continuum conservation laws from Sec. 5.2 include contributions from molecular diffusion. What is now described is a continuum in which almost all particles are neutral and uniform. A relatively small fraction of the particles are charged. For a single charged species, taken for purposes of illillustration as positive, the conservation of mass equation is Eq. 5.2.9, with G = 0 and R = 0. Combined with Gauss' law, it gives

$$\frac{\partial \rho}{\partial t} + (\vec{v} + b\vec{E})\cdot\nabla\rho = K_+ \nabla^2 \rho - \frac{\rho^2 b}{\varepsilon} \tag{1}$$

With a characteristic length ℓ and time τ, fluid velocity U and electric field E, the respective terms in Eq. 1 are of the order

$$\left(\frac{1}{\tau}\right);\quad \left(\frac{U}{\ell} \equiv \frac{1}{\tau_{trans}}\right);\quad \left(\frac{bE}{\ell} \equiv \frac{1}{\tau_{mig}}\right);\quad \left(\frac{K_+}{\ell^2} \equiv \frac{1}{\tau_D}\right);\quad \left(\frac{\rho b}{\varepsilon_o} \equiv \frac{1}{\tau_e}\right) \tag{2}$$

where the expression has been divided by a characteristic amplitude of ρ. For the charging of a particle having radius a, ℓ might be taken as a. The competition between diffusion and migration is represented by the terms in τ_{mig} and τ_D. These terms are equal if $\tau_{mig} = \tau_D$; and, because of the Einstein relation, Eq. 5.2.8, this is equivalent to

$$\ell E = kT/q \tag{3}$$

Thus, thermal diffusion and migration are of equal importance if the thermal voltage is equal to the voltage drop over a characteristic length. For $E = 10^5$ V/m (typical of fields in an electrostatic precipitator) the length that makes diffusion and migration equal is 2.5×10^{-7} m. The radius, a, of the macroscopic particle is taken as being of this order.

The diffusion time is estimated by taking as a typical ion mobility from Table 5.2.1, $b = 10^{-4}$, which (for an ion of one electronic charge) gives as a typical diffusion coefficient $K_+ = 2.5 \times 10^{-6}$. Thus, the diffusion time is only 2.5×10^{-8} sec.

By comparison, the self-precipitation time τ_e is long. Whether ions are present in a given volume by virtue of convection or migration, $\tau_e \approx 10^{-3}$ sec or longer is typical. After all, the ions are self-precipitating with this time and some other mechanism having an equally short characteristic time must be available to secure the required density.

The transport time is estimated by taking as typical the velocity of a charged submicron particle in a field of 10^5 V/m, say 10^{-2} m/sec. Thus $\tau_{trans} = 2.5 \times 10^{-5}$ sec, which is still 100 times longer than τ_D and τ_{mig}.

Consistent with ignoring the self-precipitation term is the neglect of contributions to $\vec{E}$ from the diffusing ions. Thus, $\vec{E}$ in Eq. 1 is taken as imposed, in general by the charge, Q, on the macroscopic particle and charges on external electrodes. With this understanding, and one more observation, Eq. 1 then reduces to

$$\nabla\cdot(b\vec{E}\rho - K_+\nabla\rho) = 0 \tag{4}$$

The first term in Eq. 1 has been neglected because the time scale for the charging process is very long compared to the diffusion and migration times. Looking ahead, it will be found that the charging time is of the order of τ_e. The charging process is quasi-stationary in the volume with the transient resulting only because of the field's dependence on the charge, Q, of the macroscopic particle.

In general, the solution of Eq. 4 with an externally applied electric field is difficult. Here, it will now be assumed that any ambient electric field is small compared to $(kT/q)/\ell$. Thus, in Eq. 4 the electric field is now taken as

$$\vec{E} = \frac{Q}{4\pi\varepsilon_o r^2}\vec{i}_r \tag{5}$$

With this field there is a radial symmetry, so Eq. 4 can be integrated once to obtain

$$4\pi r^2 K_+ \frac{d\rho}{dr} - \frac{bQ}{\varepsilon_o}\rho = i \tag{6}$$

Here, i(t) is the electrical current to the particle.

Superposition of particular and homogeneous solutions to Eq. 6 results in

$$\rho = \left(\rho_o + \frac{i\varepsilon_o}{bQ}\right) \exp\left[-\frac{bQ}{4\pi\varepsilon_o K_+ r}\right] - \frac{i\varepsilon_o}{bQ} \tag{7}$$

where the coefficient in front of the second term, the homogeneous solution, has been adjusted to make $\rho \to \rho_o$ far from the particle.

The diffusion model pictures ions in the neighborhood of a given point as having a random distribution of velocities. At the surface of the particle, those moving inward are absorbed and this forces the ion density there to zero. Thus, a second boundary condition is $\rho(a) = 0$ and Eq. 7 then becomes a relation between the particle charge and the rate of charging, i(t):

$$\frac{dQ}{dt} = i = \frac{b\rho_o}{\varepsilon_o}\,\frac{Qe^{-fQ}}{1 - e^{-fQ}} \tag{8}$$

where in view of the Einstein relation, Eq. 5.2.8, $f \equiv q/4\pi\varepsilon_o akT$.

Rewritten so as to be integrable, this Fuchs-Pluvinage equation[1] becomes

$$\int_o^Q \frac{e^{fQ} - 1}{Q}\,dQ = \int_o^t \frac{b\rho_o}{\varepsilon_o}\,dt \tag{9}$$

Integration then gives

$$\sum_{m=1}^{\infty} \frac{Q^m}{m\,m!} = t \tag{10}$$

where $\underline{Q} = Q/Q_D$ ($Q_D = 1/f = 4\pi\varepsilon_o akT/q$ is the charge needed to terminate the thermal "field", $(kT/q)/a$, on the surface of the particle) and where $\underline{t} = t/\tau_e$ ($\tau_e = \varepsilon_o/\rho_o b$, the self-precipitation time for the ions based on the ion density far from the particle). This charging characteristic is shown in Fig. 10.7.1.

Diffusion charging is expected to dominate over impact charging if the particle is sufficiently small that $aE < kT/q$, where E is the imposed or ambient electric field. Thus, in a field of 10^5 V/m, particles must be smaller than about 0.2 μm for diffusion charging to prevail. In fact, for the model to be valid, there is also a lower limit on size. The continuum picture of diffusion depends on the particle having a radius that is large compared to the mean free path of the ions and neutrals. In air at atmospheric pressure, this distance is 0.09 μm. For particles somewhat smaller than this, the continuum diffusion model is called into question. Models based on having a mean free path much greater than the particle radius give a charging law that is surprisingly similar to Eq. 10,[2] so the result is actually useful for particles smaller than the mean free path. Effects of the ambient field (impact charging) in combination with diffusion have been considered.[3]

---

1. N. A. Fuchs, Izv. Akad. Nauk USSR, Ser. Geogr. Geophys. 11, 341 (1947); P. Pluvinage, Ann. Geophys. 3, 2 (1947).

2. H. J. White, Industrial Electrostatic Precipitation, Addison-Wesley, Reading, Mass., 1963, pp. 137-141.

3. B. Y. H. Liu and H. C. Yeh, J. Appl. Phys. 39, 1396 (1968).

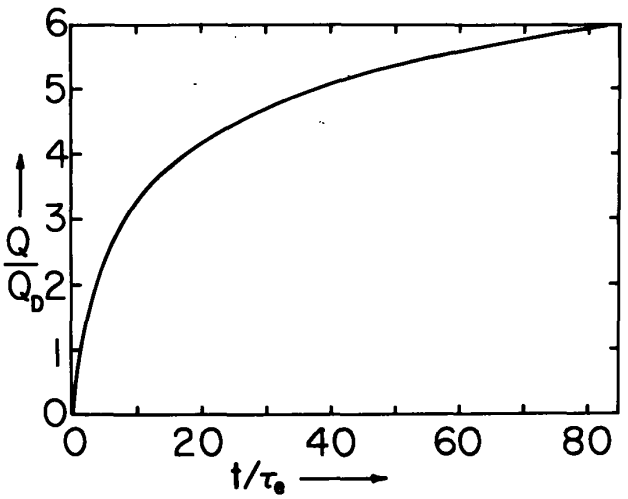

Fig. 10.7.1

Normalized charge on a macroscopic particle having radius a, as a function of normalized time, where charging is by diffusion alone, $Q_D \equiv 4\pi\varepsilon_o akT/q$ and $\tau_e \equiv \varepsilon_o/\rho_o b$.

10.8 Charge Double Layer

Considered in this section is the competition between migration and diffusion that creates a double layer at an interface between a bipolar conductor and an insulating boundary. The fluid is some form of electrolyte in which dissociation has created ion species having densities $\rho_\pm$ with a background of molecules having density n. The conservation laws for the charged and neutral species are Eqs. 5.8.9 and 5.8.10 and the system is EQS.

At the outset, the electrolyte is presumed to be highly ionized. As discussed in Sec. 5.9, this means that generation largely depletes the neutral density. In the neutral conservation equation, Eq. 5.8.10, terms on the left are essentially zero while recombination and generation on the right almost exactly balance. As a result, G-R is negligible in the charged particle equations, Eqs. 5.8.9, as well.

Consider the quasi-stationary distribution of ions in the vicinity of an insulating boundary. For now, there is no fluid convection, so $\vec{v} = 0$. The steady one-dimensional particle conservation statements then reduce to

$$\frac{d}{dx}\left[b_+E_x\rho_+ - K_+\frac{d\rho_+}{dx}\right] = 0 \tag{1}$$

$$\frac{d}{dx}\left[-b_-E_x\rho_- - K_-\frac{d\rho_-}{dx}\right] = 0 \tag{2}$$

with Gauss' law linking the electric field to the charge densities

$$\frac{d\varepsilon E_x}{dx} = \rho_+ - \rho_- \tag{3}$$

The polarizability of the fluid is assumed uniform, so ε is a constant.

The wall, at x = 0, is taken as insulating or "polarized," in that there is no current due to either species through its surface. Hence, the current densities in brackets in Eqs. 1 and 2 are each zero. These expressions are then solved for E_x. Because $\rho^{-1}d\rho/dx = d(\ell n\rho)/dx$ and $E_x = -d\Phi/dx$, it follows that

$$\Phi = -\frac{K_+}{b_+}\ln\frac{\rho_+}{\rho_o} = -\frac{kT}{q}\ln\frac{\rho_+}{\rho_o} \tag{4}$$

$$\Phi = \frac{K_-}{b_-}\ln\frac{\rho_-}{\rho_o} = \frac{kT}{q}\ln\frac{\rho_-}{\rho_o} \tag{5}$$

Here, as an integration constant, the charge densities have been taken as reaching the same uniform density, ρ_o, far from the boundary. Also, the Einstein relation, Eq. 5.2.8, has been used to express the ratio of diffusion coefficient to mobility in terms of the thermal voltage kT/q. Consistent

with the positive and negative charges being generated by an ionization is the assumption that the q is the same for each ionized species.

The charge densities required to express Gauss' law can now be found by solving Eqs. 4 and 5 for $\rho_{\pm}$. Thus, Eq. 3 becomes the classic Debye-Hückel[1] expression from which the double-layer potential is determined:

$$\frac{d^2\Phi}{dx^2} = \frac{2\rho_o}{\epsilon} \sinh [\Phi/(kT/q)] \tag{6}$$

Normalization of the potential and length makes clear the key role of the Debye length, δ_D:

$$x = \underline{x}\delta_D, \quad \Phi = \underline{\Phi}kT/q, \quad \delta_D \equiv \sqrt{\frac{\epsilon kT}{2\rho_o q}} \tag{7}$$

because then Eq. 6 becomes simply

$$\frac{d^2\Phi}{dx^2} = \sinh \Phi \tag{8}$$

The Debye length is that distance over which the potential developed by separating a charge density ρ_o from the background charge of the opposite polarity is equal to the thermal voltage kT/q. By substituting for $kT/q = K/b$, δ_D can also alternatively be considered the distance over which the molecular diffusion time δ_D^2/K is equal to the self-precipitation time $\epsilon/\rho b$. Thus, δ_D varies from about 100 Å in aqueous electrolytes to microns in semi-insulating liquids.

To integrate Eq. 8, multiply by $D\Phi$ and form the perfect differential

$$\frac{d}{dx}\left[\frac{1}{2}\left(\frac{d\Phi}{dx}\right)^2 - \cosh \Phi\right] = 0 \tag{9}$$

Far from the layer, the potential is defined as zero. Because there is no current flow there and the charge densities neutralize each other in this region, the electric field $-D\Phi$ also goes to zero far from the boundary. Thus, the x-independent quantity in brackets in Eq. 9 is unity, and the expression can be solved for $D\Phi$. The x- and Φ-dependence of that expression can be separated so that it can be integrated:

$$\int_o^x dx = \pm \int_{-\zeta}^{\Phi} \frac{d\Phi}{\sqrt{2(\cosh \Phi - 1)}} \tag{10}$$

As a function of the normalized zeta potential $\underline{\zeta}$, this result is illustrated in Fig. 10.8.1. The exponential character of the potential distribution is best seen directly from Eq. 6 by recognizing that if $\underline{\Phi} << 1$, sinh can be approximated by its argument. It follows that the solution is simply $\underline{\Phi} = -\underline{\zeta} \exp(-\underline{x})$. For $\underline{\zeta} > 1$, the rate of decay is faster than would be expected from low $\underline{\zeta}$ limit.

On the interface is a surface charge given by

$$\underline{\sigma}_f = -\frac{d\Phi}{dx}; \quad \underline{\sigma}_f = \sigma_f \sqrt{\frac{2\rho_o \epsilon kT}{q}} \tag{11}$$

and this has image charge distributed throughout the diffuse half of the double layer. Found from the potential by inverting Eqs. 4 and 5, the charge densities $\rho_{\pm}$ and net charge density ρ_f are illustrated in Fig. 10.8.2.

Double layers can exist not only at interfaces between an insulating material and an electrolyte, but even at the interface between a liquid metal such as mercury and an electrolyte. What is required is an interface that, for lack of chemical reaction, largely prevents the transfer of charge. For potential differences under about a volt or so, even a mercury-electrolyte interface can prevent the passage of current. Double layers at such interfaces are taken up in Sec. 10.11. In the next two sections, the double layer abuts a material that is itself a rigid electrical insulator.

---

1. P. Delahay, Double Layer and Electrode Kinetics, Interscience Publishers, New York, 1966, pp. 33-52.

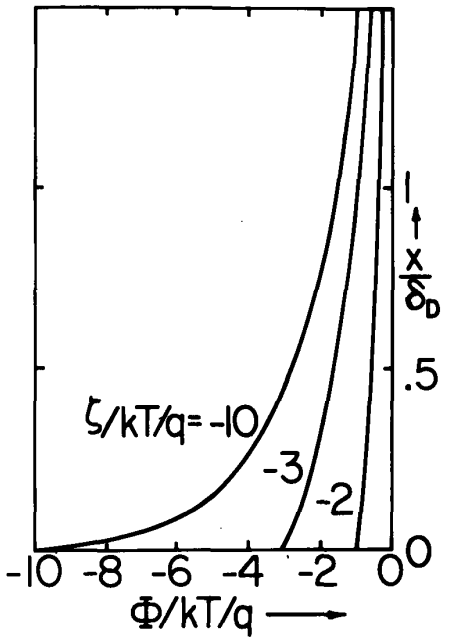

Fig. 10.8.1. Potential distribution in diffuse part of double layer with zeta potential as parameter.

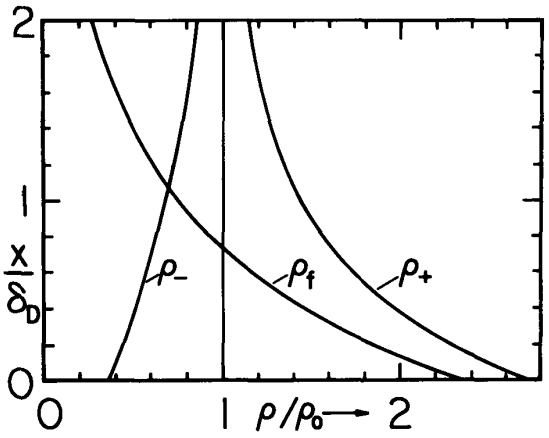

Fig. 10.8.2. Charge density distributions for $\zeta = kT/q$.

10.9 Electrokinetic Shear Flow Model

A double layer in an electrolyte abuting an insulating solid is sketched in Fig. 10.9.1. Even though this layer tends to be extremely thin, the application of an electric field tangential to the boundary can result in a significant relative motion between the solid and fluid. From the boundary frame of reference, the field E_y exerts a force density $\rho_f E_y$ on the fluid, and shear flow results. Because pressure forces prevent motion in the x direction, flow is essentially orthogonal to the double-layer diffusion and migration currents. Thus it can be superimposed on the static double-layer distribution discussed in Sec. 10.8. In layers that are "wrapped around" a particle, as taken up in Sec. 10.10, a component of the applied field tends to compete with the fields internal to the layer. The model now developed can only be applied to such situations if the x component of the applied field is small compared to the double-layer internal field.

The relative flow is inhibited by the viscous stresses associated with strain rates developed within the layer itself. These strain rates are inversely proportional to the layer thickness (of the order of the Debye length) so the relative velocity tends to be small. Nevertheless, such electrokinetic flows are important in fine capillaries and in the interstices of membranes. Electrophoretic motions of both macroscopic and microscopic particles in electrolytes also have their origins in this streaming.

The simple model developed now is used in this section to describe electro-osmosis through pores. It will be used to describe electrophoresis of particles in Sec. 10.10.

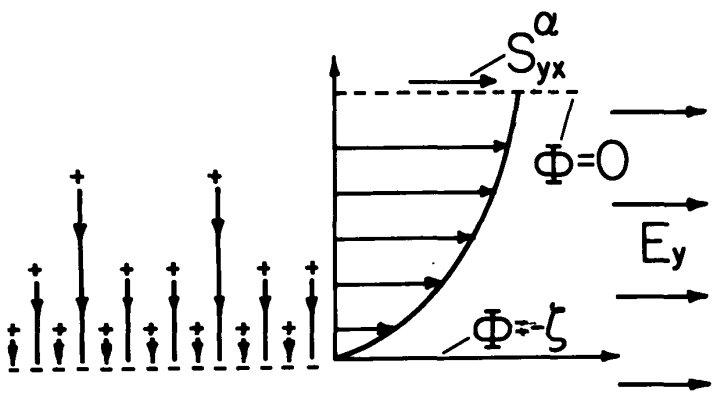

Fig. 10.9.1

Schematic view of double layer subject to imposed field in y direction resulting in shear flow.

Zeta Potential Boundary Slip Condition: For flows that have a scale that is large compared to the Debye thickness, the electromechanical coupling can be reduced to a quasi-one-dimensional model that amounts to a boundary condition for the flow.

On the scale of the double layer, the imposed electric field can be considered to be uniform. The velocity is fully developed in its distribution in the sense of Sec. 9.3. Also, because the double-layer region is so thin, the viscous force density far outweighs the pressure gradient in the y direction. Thus, the force equation, Eq. 9.3.4, takes the one-dimensional form

$$\eta \frac{d^2 v_y}{dx^2} = -\frac{dT_{yx}}{dx}; \quad T_{yx} = \varepsilon E_y E_x \tag{1}$$

where the derivative of the shear component of the stress tensor simply represents the force density $\rho_f E_y$. To prescribe the flow outside the layer, it is assumed that at the distance d from the slip plane, there is a fictitious plane at which fluid moves with the velocity $v_y^\alpha \vec{i}_y$ and sustains a viscous shear stress S_{yx}^α.

The constant from integration of Eq. 1 is evaluated by recognizing that the electric shear stress falls to zero at x = d, where the external viscous stress equilibrates the internal stress:

$$\eta \frac{dv_y}{dx} = -T_{yx} + S_{yx}^\alpha \tag{2}$$

A second integration is possible because E_y is constant and $E_x = -d\Phi/dx$. Also, S_{yx}^α is a constant, so that

$$\begin{aligned} \eta v_y &= \int_o^x \varepsilon E_y \frac{d\Phi}{dx} dx + \int_o^x S_{yx}^\alpha dx \\ &= \varepsilon E_y [\Phi(x) - \Phi(0)] + x S_{yx}^\alpha \end{aligned} \tag{3}$$

In terms of the conventions used in Sec. 10.9, the potential of the slip plane is taken as $-\zeta$, while that at x = d is zero, so Eq. 3 becomes

$$v_y^\alpha = \frac{\varepsilon E_y \zeta}{\eta} + \frac{d}{\eta} S_{yx}^\alpha \tag{4}$$

If the external stress, S_{yx}^α, comes from shear rates determined by flow on a scale large compared to δ_D, the last term in Eq. 4 can be ignored. The mechanical boundary condition representing the double layer is then simply

$$v_y = \frac{\varepsilon E_y \zeta}{\eta} \tag{5}$$

In refining the simple model, a distinction is sometimes made between the potential evaluated in the slip plane and evaluated on the other side of a compact zone of charge that forms part of the double layer but is not in the fluid and hence cannot move.

Electro-Osmosis: Flow through a planar duct, such as shown in Table 9.3.1, illustrates the application of Eq. 4. Suppose that the duct width, Δ, is much greater than a Debye length. In the volume of the flow, there are no electrical stresses, so Eq. (a) of Table 9.3.1 gives the velocity as

$$v_y(x) = \frac{\varepsilon E_y \zeta}{\eta} + \frac{\Delta^2}{2\eta} \frac{\partial p'}{\partial y} \left[\left(\frac{x}{\Delta}\right)^2 - \frac{x}{\Delta} \right] \tag{6}$$

The volume rate of flow per unit z follows as

$$Q_v = -\frac{\Delta^3}{12\eta} \frac{dp}{dy} + \frac{\varepsilon E_y \zeta}{\eta} \Delta \tag{7}$$

This relation gives the trade-off between flow rate and pressure drop of an electrokinetic pump. The pressure rise developed in a length ℓ of the pore is at most that for zero flow rate,

$$\Delta p = \varepsilon E_y \zeta \ell / \Delta^2 \tag{8}$$

In situations where Δ is small (but, to validate the model, still larger than a Debye length), this pressure can be appreciable. For example, with $\zeta = 0.1$ V (about four times the thermal voltage kT/q), $\Delta = 1$ μm, $E_y = 10^4$ V/m, $\ell = 0.1$ m and $\epsilon \approx 5\epsilon_o$, the pressure rise is about 5 x 10^4 n/m^2, which would raise water to a height of about ~~0.5~~ 50 m.

In membranes composed of a matrix of materials, perhaps of a biological origin, surrounded by double layers, flow of fluid through the interstices is modeled as flow through a system of pores, each described by a relation such as Eq. 7.[1] The velocity profile for δ_D arbitrary relative to Δ is found in Prob. 10.9.1.

Electrical Relations; Streaming Potential: Associated with the electric field and flow in the y direction, there is a current density

$$J_y = (\rho_+ b_+ + \rho_- b_-)E_y + (\rho_+ - \rho_-)v_y \tag{9}$$

The charge densities in this expression are as found in Sec. 10.8 and illustrated by Fig. 10.8.2. The conductivity, $\rho_+ b_+ + \rho_- b_-$, tends to remain uniform through the double layer, but, if $\zeta > 1$, tends to be increased somewhat over the bulk value. The convection term is concentrated in the region of net charge, and hence (on the scale of an external flow having characteristic lengths large compared to δ_D) comprises a surface current. Because it results from motion of the fluid, it might be termed a convection current. However, it results from fluid motion within a Debye length or so of the boundary, and this motion is caused by the externally applied pressure difference and the field itself. For a small zeta potential $\sinh \underline{\Phi} \simeq \underline{\Phi}$ and $\Phi \simeq -\zeta \exp(-x/\delta_D)$, and so it follows from Eqs. 10.8.4 and 10.8.5 that

$$\rho_+ - \rho_- = -\frac{2\rho_o}{(kT/q)}\Phi = \frac{2\rho_o\zeta}{kT/q}\exp(-x/\delta_D) \tag{10}$$

and that the velocity of Eq. 3 is

$$v_y = \frac{\epsilon E_y}{\eta}\zeta[1 - \exp(-x/\delta_D)] + \frac{x}{\eta}S^{\alpha}_{yx} \tag{11}$$

The current density of Eq. 9 can be divided into a volume density represented by the first term evaluated with $\rho_+ \simeq \rho_o$ and a surface current density represented by the second term

$$K_y = \int_o^\infty (\rho_+ - \rho_-)v_y dx = \int_o^\infty \frac{2\rho_o\zeta}{kT/q}e^{-x/\delta_D}\left[\frac{\epsilon E_y \zeta}{\eta}(1 - e^{-x/\delta_D}) + \frac{xS^{\alpha}_{yx}}{\eta}\right]dx$$
$$= \frac{2\rho_o\zeta}{\eta(kT/q)}\left(\frac{\zeta\epsilon\delta_D}{2}E_y + \delta_D^2 S_{yx}\right) \tag{12}$$

Both terms in this surface current density are due to convection, but the first reflects motion caused by the field itself. This contribution therefore appears much as if the material had a surface conductivity $\rho_o\zeta^2\epsilon\delta_D/\eta(kT/q)$. Its origins are more apparent if it is recognized as the product of the surface charge $\rho_o\delta_D\zeta/(kT/q)$ and the slip velocity $\epsilon\zeta E_y/\eta$.

The total current, i (per unit length in the z direction), flowing through a channel having width Δ is then the sum of the surface currents at each of the walls and the bulk current

$$i = \sigma\Delta E_y + 2K_y \tag{13}$$

where K_y is given by Eq. 12. For the case at hand where $\Delta >> \delta_D$, the wall stress, S_{yx}, can be approximated using Eq. 5 as a boundary condition, and so is determined by the pressure gradient. (See Prob. 10.9.2.)

10.10 Particle Electrophoresis and Sedimentation Potential

Electrophoretic motions account for the "migration" of a wide variety of particles in an applied electric field intensity. Particles may be as small as large molecules or as large as macroscopic particles (in the micron-diameter range). If these motions persist over times much longer than the charge relaxation time, it is clear that the particle and its immediate surroundings carry no net charge. The particle is not pulled through the fluid by the electric field, but rather by dint of the field "swims" through the fluid.

---

1. A. J. Grodzinsky and J. R. Melcher, "Elecromechanical Transduction with Charged Polyelectrolyte Membranes," IEEE Trans. on Biomedical Eng., BME-23, No. 6, 421-33 (1976).

Electrophoresis is used by chemists as a means of classifying particles. For example, protein molecules can be distinguised by electrophoretic techniques, and the electrophoretic motion of particles through a liquid absorbed in paper or comprising the main constituent of a gel is used for routine clinical tests (paper and gel electrophoresis). Electrophoretic motions are also used to control particles of pigment in liquids, for example in large-scale painting of metal surfaces.

Electrophoretic motions are now modeled under the assumption that the particle is much larger in its extreme dimensions than the thickness of the double layer. The particles are insulating, and approximated as spherical with a radius R, as shown in Fig. 10.10.1. The particle is taken as fixed, with the fluid having a uniform relative flow at $z \to \pm\infty$, as illustrated. External electrodes are used to apply the electric field intensity E_o, which is also uniform in the z direction. As $z \to \pm\infty$,

$$\Phi \to -E_o r \cos\theta$$
$$\vec{v} \to U\vec{i}_z \qquad (1)$$

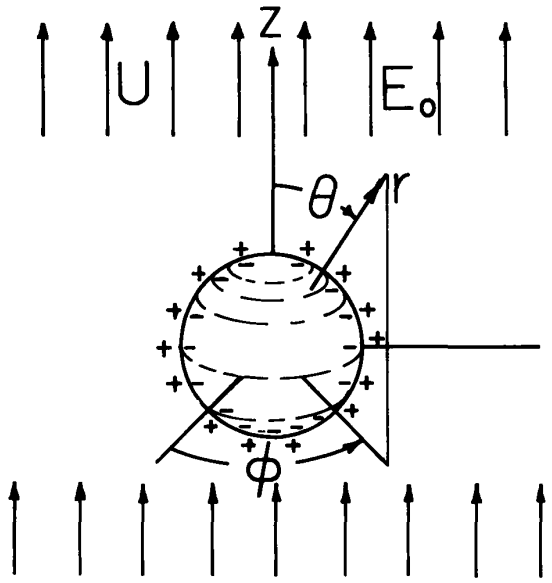

Fig. 10.10.1. Solid insulating particle supporting double layer.

Electric Field Distribution: For a control volume which cuts through the double layer, as shown in Fig. 10.10.2, conservation of charge requires that the conduction current from the bulk of the liquid be balanced by the divergence of convection surface current along the interface:

$$\vec{n}\cdot\vec{J}_f + \nabla_\Sigma\cdot\vec{K}_f = 0 \qquad (2)$$

Here, $\vec{K}_f$ is the integral of the tangential current density $\rho_f\vec{v}$ over the mobile part of the double layer and takes the form of Eq. 10.9.11. It is assumed that, because the external viscous stress results from strain rates on the scale of R, and relative motions of the liquid are due to the field itself, the stress term in Eq. 10.9.12 is negligible compared to the first term. In terms of the spherical coordinates, Eq. 2 therefore requires that at r = R,

$$-\sigma\frac{\partial\Phi}{\partial r} + \frac{1}{R\sin\theta}\frac{\partial}{\partial\theta}(\sigma_s E_\theta \sin\theta) = 0 \qquad (3)$$

where $\sigma_s \equiv \rho_\infty \zeta^2 \epsilon\delta_D/\eta(kT/q)$. To satisfy the condition on Φ at infinity, Eq. 1, Φ is taken as having the form

$$\Phi = -E_o r\cos\theta + A\frac{\cos\theta}{r^2} \qquad (4)$$

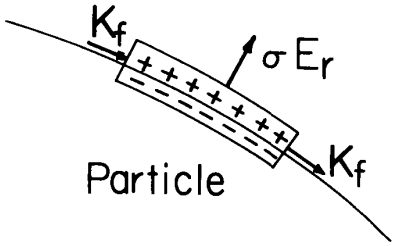

Fig. 10.10.2. Control volume enclosing double layer.

It follows from Eq. 3 that

$$A = -\frac{E_o R^3}{2}\frac{[\sigma - \frac{2\sigma_s}{R}]}{[\sigma + \frac{\sigma_s}{R}]} \qquad (5)$$

and hence that at r = R,

$$E_\theta = -\frac{3E_o\sigma}{2(\sigma + \frac{\sigma_s}{R})}\sin\theta \qquad (6)$$

What has been solved has the appearance of being an electrical conduction problem. But, remember that the surface conductivity reflects the convection of net charge by the slip velocity of the fluid relative to the particle.

Fluid Flow and Stress Balance: The slip velocity follows from Eq. 10.9.3 evaluated using Eq. 6:

$$v_\theta = \frac{\varepsilon\zeta}{\eta} E_\theta = \tilde{v}_\theta \sin\theta; \quad \tilde{v}_\theta \equiv -\frac{3}{2}\frac{\varepsilon\zeta}{\eta}\frac{E_o}{1+\frac{\sigma_s}{\sigma R}} \tag{7}$$

In addition to this boundary condition, the radial velocity is essentially zero at r = R and the velocity approaches the uniform one of Eq. 1 far from the particle. Because of the small particle size and relatively low velocities, the conditions for low Reynolds number are likely to prevail.

The boundary conditions fit the exterior, n=1, high Reynolds number flows of Table 7.20.1. Thus, the stress components follow directly from Eq. 7.20.24 evaluated using Eq. 7 and $v_r = 0$:

$$\begin{bmatrix} \tilde{S}_{rr} \\ \tilde{S}_{\theta r} \end{bmatrix} = -\frac{\eta}{R}\begin{bmatrix} \frac{9}{2} & \frac{3}{2} \\ 3 & 3 \end{bmatrix}\begin{bmatrix} -\frac{U}{2} \\ \tilde{v}_\theta + U \end{bmatrix} \tag{8}$$

Here the complex amplitudes represent the θ dependence summarized in Table 7.20.1.

The net force on the particle in the z direction can be computed from these stresses by integrating the appropriate components over the spherical surface, as in Eq. 7.21.1:

$$f_z = \frac{8}{3}\pi R^2(\tilde{S}_{rr} - \tilde{S}_{\theta r}) = 4\pi R\eta(6U + 4\tilde{v}_\theta) \tag{9}$$

There are no external forces acting on the particle, so $f_z = 0$. It therefore follows from Eq. 9 that the particle "swims" at a velocity

$$U = -\frac{2}{3}\tilde{v}_\theta = \frac{\varepsilon\zeta}{\eta}\frac{E_o}{1+\frac{\sigma_s}{\sigma R}} \tag{10}$$

where $\sigma_s \equiv \rho_q \zeta^2 \varepsilon\delta_D/\eta(kT/q)$. This velocity is now interpreted as the velocity of the particle due to an applied field with the fluid stationary. Note that it is in a direction opposite to that of the applied field (assuming that the zeta potential is positive, or that the charge in the liquid is positive, as indicated in Fig. 10.10.1). The charges in the fluid surrounding the particle carry the fluid in the direction of the field. The resulting force on the particle is in an opposite direction. The particle moves as if it were subject to the net force QE, where Q is proportional to the net charge on the particle side of the double layer.

As would be expected, for small zeta potentials, the particle velocity increases with ζ. However, as ζ becomes "large," this velocity peaks and finally becomes inversely proportional to ζ. This finding might at first seem surprising, but relates to the fact that for large ζ, the motion is impeded by fields generated by the build-up of charge carried forward by convection. According to the model, convected charge must be carried back again by conduction through the surrounding liquid. Thus it is that the tendency of an increasing ζ to decrease the particle mobility is avoided by increasing the conductivity of the surrounding fluid.[1]

With external forces such as those due to gravity or centrifugal acceleration forcing a particle through the liquid, reciprocal coupling occurs. Convection of charge in the double layer results in a dipole of electric field intensity and current density around the particle. If many particles are present, these generated fields add, to induce a "macroscopic" field measurable by electrodes immersed in the liquid through which the collection of particle move. This sedimentation potential (or "Dorn effect") is the subject of Prob. 10.10.3.

10.11 Electrocapillarity

A simple experiment that would prove baffling without an appreciation for the action of double layers at interfaces between liquids is sketched in Fig. 10.11.1. Mercury drops fall from a pipette

1. For extensive discussion see V. G. Levich, Physicochemical Hydrodynamics, Prentice-Hall, Englewood Cliffs, N.J., 1963, pp. 472-93.

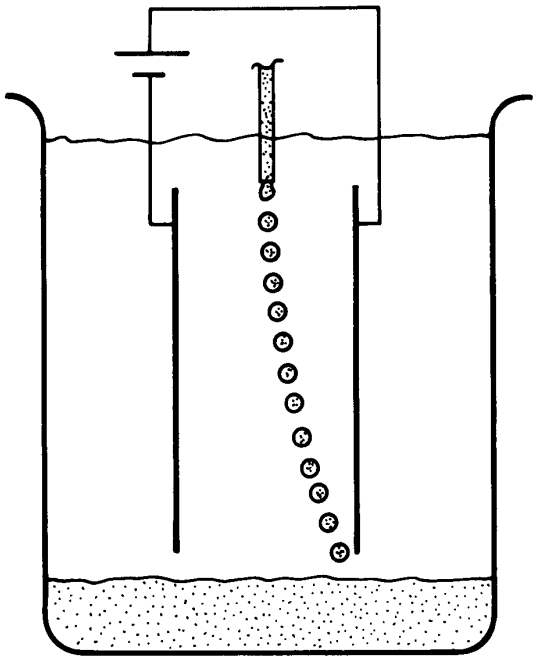

Fig. 10.11.1

Falling mercury drops surrounded by NaCl electrolyte are deflected as they pass through imposed field E_o. Typical for a drop having radius R = 1 mm passing through field of E_o = 100 V/m would be a horizontal velocity of 5 cm/sec.

through an electrolyte between electrodes to which a potential difference of a few volts has been applied. The drops are strongly deflected to one of the electrodes.

It is natural to simply attribute a net charge to each drop. However, the electrolyte is relatively conducting and this means that any net charge would leak away in a few relaxation times (Prob. 5.10.3). For the experiment of Fig. 10.11.1 this time is about 10^{-8} sec! Clearly, the drop and its immediate surroundings can carry no net charge on the time scale of the experiment. The drops must be "swimming," much as for the electrophoresing particles of Sec. 10.10. However, there are two important ways in which the drops do not fit the electrophoresis model. First, the drop is much more conducting than its surroundings. More important, it moves much too fast to be accounted for by the electrophoresis model and reasonable zeta potentials.

Up to potential differences on the order of a volt or so, the mercury-electrolyte interface can be polarized, in the sense that there are no chemical reactions to sustain a current flow so that the interface acts as an insulator. The result is an electric field within the double layer that is far larger than that in the electrolyte, on the order of 10^8 V/m compared to 10^2 V/m. The conditions are established for having a double-layer surface force density, as discussed in Sec. 3.11.

If the drops were rigid, the surface force density would have no effect. On a closed surface, there is no net force resulting from a surface force density (Prob. 3.11.2). However, the liquid surface can be set into motion. The shear rate is determined by the scale of the drop and not the scale of the double layer. This is why the drops move with such surprising speed relative to particles subject to electrophoresis.

The double layer also provides a mechanism for mechanical-to-electrical transduction. In the mercury drop experiment, electrical signals are generated in the electrolyte by the passing drops. Here again is cause for surprise, because generation of an appreciable electric field by the motion implies a significant electric Reynolds number. Based on the bulk properties of the electrolyte and the time for a drop to migrate one radius, this number is typically 10^{-7}. The lesson here is that the relevant relaxation time should reflect the heterogeneity of the system. The electric energy storage is in the double layer but the electrical loss is in the surrounding medium. Hence, the correct electric Reynolds number is modified by the ratio of the drop radius to the double layer thickness, a number that is of the order of $10^{-3}/10^{-8} = 10^5$. Drop motions are taken up in Sec. 10.12.

That the double layer electric surface force density of Sec. 3.11 takes a form similar to that found in Sec. 7.6 for surface tension, is a warning that in dealing with naturally occurring double layers it is not possible to make a clear distinction between electrical and mechanical surface force densities. The microstructure of the fields within the layer is in general not known. For example, through the electrochemical interaction of mercury and electrolyte, interior fields are generated which can be altered by an externally applied potential difference, but are not solely determined by external constraints.

Developments in this section make no distinction between electrical and mechanical surface forces. Rather, a surface tension γ_e is used to represent both electrical contributions and those ordinarily associated with the surface tension. The starting point is a statement of conservation of energy for an element of the interface. Such a statement defines the energy in terms of the local geometry and potential of the interface. If the exterior field contribution to the energy of the system is significant, then the energy stored in the electric field is a function of the geometry of the interface and of neighboring conductors and dielectrics. This contribution of the exterior fields is represented by the first term in Eq. 3.11.8. In what follows, it is assumed that exterior energy storage is negligible.

The surface tension γ_e is to the interface what the stress is to the volume. With the understanding that $\gamma_E \to \gamma_e$, the control volume of Fig. 3.11.1 is used, where γ_e is visualized as a force per unit length acting normal to the edges. Because the interface can be expected to have properties independent of rotations about the normal vector $\vec{n}$, it is assumed at the outset that the surface tension acting in the μ direction is the same as that acting in the ζ direction. Also, the edges are pictured as free of interfacial shear stresses. (A monomolecular interfacial film, residing on the interface as a distinguishable phase, can behave as two-dimensional fluid or solid. For the former, γ_e is replaced by a two-dimensional tensor γ_{ij}, with components departing from the diagonal form $\gamma_{ij} = \gamma_e\delta_{ij}$ used here because of relative motion (because of surface viscosity). The role played by the pressure in the mechanical three-dimensional force density is taken by γ_e on the surface. The scalar surface tension can be regarded as an inviscid model for the interface that is particularly appropriate if the interface is clean.[2]

Force equilibrium for the control volume requires that Eq. 3.11.8 relate the surface force density and the surface tension:

$$\vec{T} = -\vec{n}\gamma_e\left[\frac{1}{R_1} + \frac{1}{R_2}\right] + \nabla_\Sigma\gamma_e \tag{1}$$

where external stress contributions are dropped.

With the objective of relating γ_e to the double-layer charge, consider conservation of energy for a uniform section of the interface. An incremental increase in the energy W_s stored in the section of interface having area A can either be caused by doing work by means of the surface stress along the edges, or by increasing the total double layer charge q_d placed on the electrolyte side of the interface in the face of the potential difference v_d:

$$\delta W_s = \gamma_e\delta A + v_d\delta q_d \tag{2}$$

The mechanical and electrical work in this expression make it analogous to the conservation of energy statement for a lumped parameter electroquasistatic coupling system, for example Eq. 3.5.1. One difference is that in Chap. 3 the force is assumed to be of purely electrical origin.

A second useful connection is between Eq. 2 and similar thermodynamic relations used in Sec. 7.22 for compressible fluids. In the volumetric deformations of a gas, $p\delta V$ plays a role analogous to that of the term $\gamma_e\delta A$ in Eq. 2.

With the objective of using the double layer potential difference v_d as an independent variable, recognize that $v_d\delta q_d = \delta(v_dq_d) - q_d\delta v_d$ so that Eq. 2 becomes

$$\delta W_s' = -\gamma_e\delta A + q_d\delta v_d; \quad W_s' \equiv q_dv_d - W_s \tag{3}$$

where W_s' is an electrocapillary coenergy function. In a manner familiar from Sec. 3.5, the assumption that W_s' is a state function of A and v_d makes it possible to write

$$\delta W_s' = \frac{\partial W_s'}{\partial A}\delta A + \frac{\partial W_s'}{\partial v_d}\delta v_d \tag{4}$$

and to conclude by comparing Eqs. 3 and 4 that

$$\gamma_e = -\frac{\partial W_s'}{\partial A}; \quad q_d = \frac{\partial W_s'}{\partial v_d}; \quad \frac{\partial\gamma_e}{\partial v_d} = -\frac{\partial q_d}{\partial A} \tag{5}$$

---

2. For discussion, see for example G. L. Gaines, Jr., The Physical Chemistry of Surface Films, Reinhold Publishing Corp., New York, 1952.

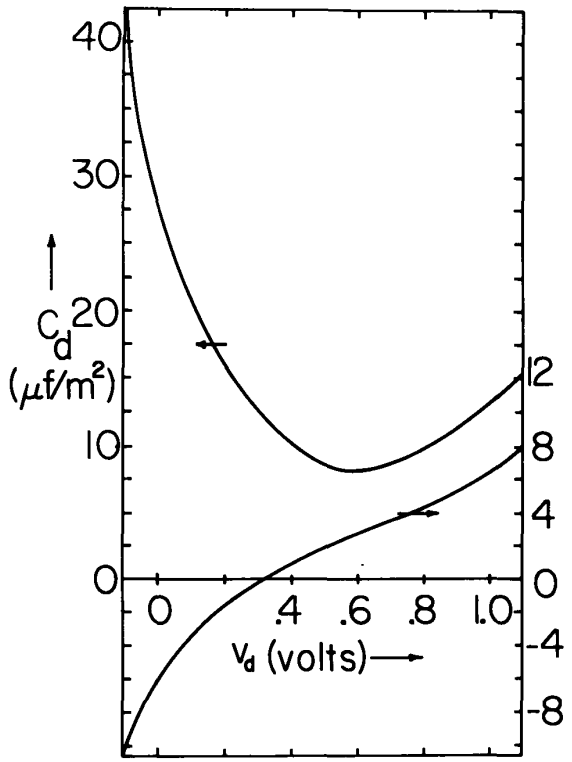

Fig. 10.11.2a. Incremental capacitance and charge per unit area as function of voltage for mercury-KNO_3. Here the electrolyte is 0.2 M KNO_3 in gel. This solid-liquid interface exhibits properties typical of liquid-liquid interfaces.[3]

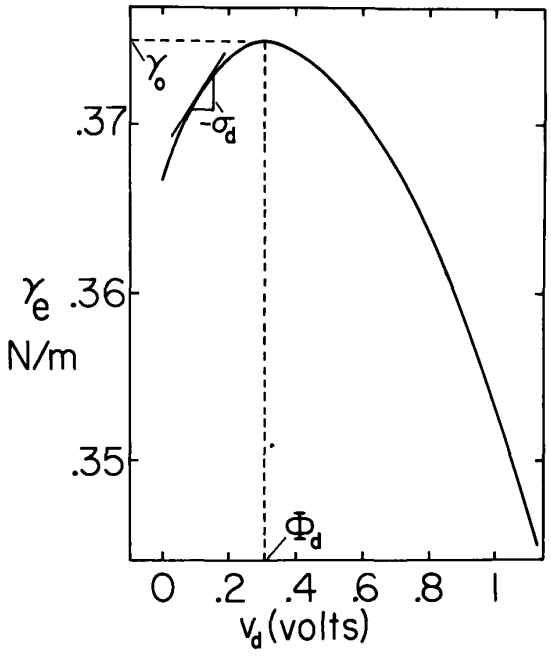

Fig. 10.11.2b. Surface tension as function of voltage for data of (a). γ_o has been defined as value for H_2O-Hg interface.

The third of these expressions follows by taking cross-derivatives of the previous two expressions.

An example of a constitutive law expressing the dependence of the charge on A is

$$q_d = A\sigma_d(v_d) \tag{6}$$

This expression pertains to a "clean" interface because it stipulates that provided the potential difference is held fixed, increasing the area of exposure between mercury and electrolyte proportionately increases the total charge. Such a law would not apply if, for example, the layer were a thin region of insulating liquid that conserved its mass and therefore thinned out as the area increased.

With the use of Eq. 6, Eq. 5c becomes the Lippmann equation:

$$-\sigma_d = \frac{\partial \gamma_e}{\partial v_d} \tag{7}$$

The graphical significance of Eq. 6 for an electrocapillary curve is depicted by Fig. 10.11.2.[3] double-layer charge/unit area determined from γ_e by Eq. 7 does not depend on a specific model.

That an alternative view has been taken of the same type of surface force density treated in Sec. 3.11 is illustrated by taking the coenergy stored in the area A as being proportional to that area and the integral of a coenergy density over the cross section of the layer,

$$W_s' = A \int_{o^-}^{o^+} W'(v)dv$$

3. A. J. Grodzinsky, "Elastic Electrocapillary Transduction," M.S. Thesis, Department of Electrical Engineering, Massachusetts Institute of Technology, Cambridge, Mass., 1971.

Then, with the use of Eq. 5a, an expression is obtained for γ_e comparable to that for γ_E given with Eq. 3.11.8. Of course, here W' can include contributions of a mechanical origin, whereas in Sec. 3.11 it does not. To preserve the generality inherent to Eq. 3, it is integrated along the state space contour of Fig. 10.11.3:

$$W_s' = -\int_{A_o}^{A} \gamma_o \delta A + A\int_{\Phi_d}^{v_d} \sigma(v_d)\delta v_d \tag{9}$$

where an electrical "clean-interface" constitutive law, Eq. 6, is assumed. The surface tension is defined as γ_o with the potential equal to Φ_d. Thus, measurement of σ_d and integration is one procedure for determining γ_e, which by virtue of Eqs. 5a and 9 is

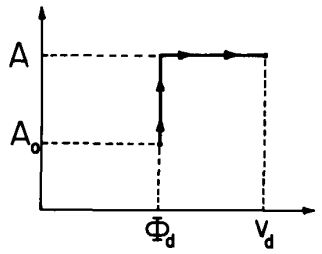

Fig. 10.11.3. Line integration in state space (A,v_d) to determine co-energy function, Eq. 9.

$$\gamma_e = \gamma_o - \int_{\Phi_d}^{v_d} \sigma_d(v_d)\delta v_d \tag{10}$$

Conventionally, σ_d is determined by electrical measurements. With the area held fixed, a section of the interface is driven by a voltage composed of a constant part V_d and a small perturbation v_d'. The measured current is then to linear terms

$$i_d = AC_d \frac{dv_d}{dt}; \quad C_d \equiv \frac{\partial \sigma_d}{\partial v_d}(V_d) \tag{11}$$

so that the incremental capacitance $C_d(v_d)$ can be deduced. The surface charge then follows from the integration:

$$\sigma_d = \int_{\Phi_d}^{v_d} C_d(V_d)dV_d \tag{12}$$

The constant of integration must be independently determined, say by measuring the voltage at which there is no mechanical linear response to a tangential perturbation field. Thus, the electrocapillary curve can be determined by two successive integrations, the first Eq. 12 and the second Eq. 10. An independent measurement of the surface tension, say at the voltage for zero charge, Φ_d, is required for the second integration constant. The three curves for the differential capacitance, C_d, double layer charge density σ_d, and surface tension γ_e are illustrated in Fig. 10.11.2.

Finally, note that for a clean interface the double-layer shear force density can still be thought of as the product of σ_d and the tangential electric field on the electrolyte side. This is seen by combining the potential and tangential field boundary conditions of Eqs. 2.10.10 and 2.10.11 (with $E_t = 0$ and Φ = constant on the metal side of the interface) to write

$$\vec{E}_t = -\nabla_\Sigma v_d \tag{13}$$

Then, if γ_e varies only by virtue of v_d,

$$\nabla_\Sigma \gamma_e = \frac{\partial \gamma}{\partial v_d}\nabla_\Sigma v_d = \sigma_d E_t \tag{14}$$

This expression for the shear component of $\vec{T}$ applies if the layer is homogeneous in the sense that any section of the interface is characterized by the same constitutive law, Eq. 8.

Electrocapillary phenomena illustrate how double layers can impart a net electric surface force density to an interface. Although most studied and best understood for H_g-electrolyte interfaces,[4] electrocapillarity serves as a thought provoking example in developing models involving other more complex combinations of materials.

4. P. Delahay, Double Layer and Electrode Kinetics, Interscience Publishers, New York, 1966.

10.12 Motion of a Liquid Drop Driven by Internal Currents

Although incapable of causing a net electric force on a closed surface, the double-layer contributions to the surface force density can nevertheless induce net motion. The specific example used to illustrate how is depicted by Fig. 10.12.1, and intended as a primitive model for the transduction of an electrochemically generated current into net mechanical migration. Perhaps it might pertain to the locomotion of a biological entity. With the driving current outside rather than inside, it is the configuration of the dropping mercury electrode. (See Prob. 10.12.1.)

The spherical double-layer interface separates an electrolytic fluid inside from a relatively highly conducting fluid outside. At the center, there is a current source having the nature of a battery, modeled here as a dipole current source. A source of I amps is separated along the z axis by a distance $d \ll R$ from a sink of I amps (the positive and negative terminals of the battery). The objective is to determine the velocity of the drop relative to the surrounding fluid, which is stationary at infinity. So that the flow is steady, use is made of a frame of reference fixed to the center of the drop. The surrounding fluid then appears to have a uniform velocity $U\vec{i}_z$ far from the drop.

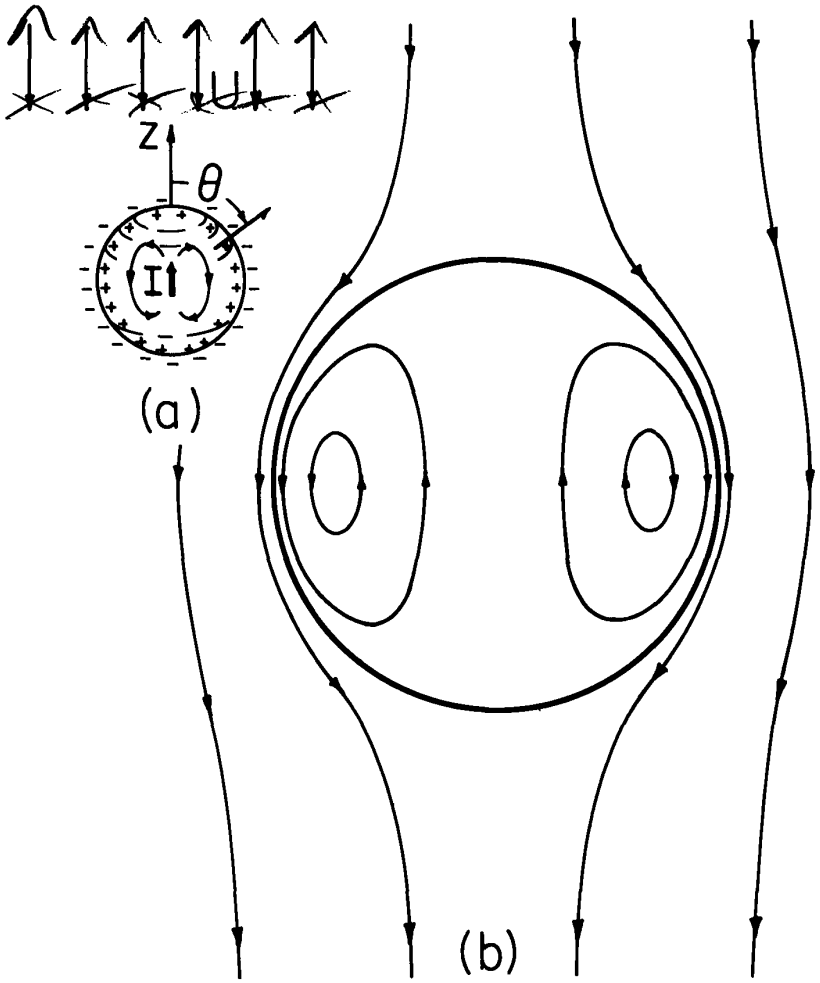

Fig. 10.12.1. (a) Liquid drop separated from surrounding liquid by ideally polarized double layer. Dipole current source is located at drop center. (b) Stream lines for fluid motion as viewed from frame fixed to drop.

With the double layer positive on the inside and I positive, U will be found to be negative, meaning that the drop is propelled in the z direction or in the direction of the dipole. Thus the magnitude and direction of migration is determined by the dipole. The physical mechanism is the double-layer shear surface force density tending to propel the interface from north to south. This density is largest at the equator. The consequent bulk flow is sketched in Fig. 10.12.1b. Inside, a doughnut-

shaped cellular motion results, while outside fluid is pumped in the -z direction. Viscous shear stresses at the interface are typically determined by the interfacial velocity and a characteristic distance on the order of the drop radius R. The double-layer thickness is many times smaller than R, and hence the viscous shear stresses within the double layer (which are based on the thickness of the double layer) make the layer move essentially as a whole. Thus, for the present purposes, the fluid velocity is continuous through the double layer, and it is the net surface force density discussed in Sec. 3.11 that is the drive.

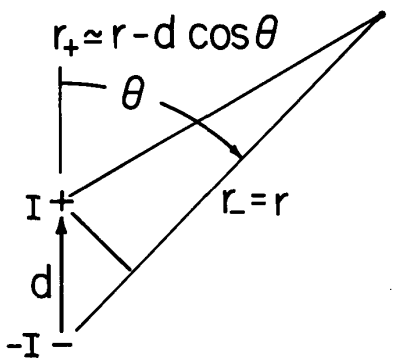

Fig. 10.12.2. Definition of dipole current source in terms of a source and sink of current disposed along the z axis a distance d apart.

The physical explanation for the drop motions applies (turned inside out) to the drop motions discussed in Prob. 10.12.1. It is because the interface can flow that the drops sustain a net electrically driven motion. Propulsion of a boat is in a way analogous. The double layer simply "rows" the drop through the surrounding fluid.

A self-consistent model for radial and tangential stress equilibrium, as well as conservation of double-layer charge, could in general be complicated. The remarkable fact is that a relatively simple model can be formulated combining electrical and mechanical distributions that have the θ dependence cos θ or sin θ. The drop is assumed to remain spherical. The assumption is subsequently shown to be valid.

First, the electrical current-dipole is represented. In the electrolyte, the current density is given by $\vec{J}_f = -\sigma_b \nabla\Phi$ and hence there is an electric potential associated with the point current source and sink, $\Phi_\pm = \pm I/4\pi\sigma_b r_\pm$. The distances $r_\pm$ are sketched in Fig. 10.12.2. By taking the limit $d \ll r$ of the superimposed source and sink potential, it is seen that in the neighborhood of the origin, the potential must be

$$\Phi \to \frac{Id}{4\pi\sigma_b}\frac{\cos\theta}{r^2} \tag{1}$$

On a spherical surface radius $c \ll R$, the potential takes the form $\mathrm{Re}\tilde{\Phi}^c \cos\theta$, which is the $n = 1$ and $m = 0$ case from Table 2.16.3. The complex amplitude on the $\beta \to c$ surface surrounding the dipole at $r = c$ is

$$\tilde{\Phi}^c = \frac{Id}{4\pi\sigma_b c^2} \tag{2}$$

The electric transfer relation, Eq. (a) from Table 2.16.3, again in the limit $c \ll R$, then gives the radial field at $r = R$ in terms of the current drive and the potential at the interface:

$$\tilde{E}_r^b = -\frac{\tilde{\Phi}^b}{R} + \frac{3c^2}{R^3}\tilde{\Phi}^c = -\frac{\tilde{\Phi}^b}{R} + \frac{3Id}{4\pi\sigma_b R^3} \tag{3}$$

The θ dependence is recovered by multiplying by cos θ.

The region $r > R$ is highly conducting, so for now the potential there is taken as uniform. The coupling at the interface is a two-way one.

Charge Conservation: Because the interface moves in a nonuniform fashion, charge carried by convection must be supplied by conduction at one pole and similarly removed at the other. The interface is presumed to be ideally polarized, so that charge conservation requires an equilibrium between the convection of the double-layer charge associated with the interior region and conduction normal to the interface from the interior:

$$\nabla_\Sigma (\sigma_d \vec{v}^b) = \frac{1}{R\sin\theta}\frac{\partial}{\partial\theta}\left[\sigma_d v_\theta^b \sin\theta\right] = \sigma_b E_r^b \tag{4}$$

A similar relation applies to the exterior side. In the absence of the electrical drive, the interface has a uniform charge σ_o consistent with a potential difference V_d. The surface potential variation caused by I is reflected in a charge variation. In the following it is assumed that the total departure of the potential from V_d is relatively small so that the double layer charge, σ_d, in Eq. 4 can be approximated by σ_o.

The transfer relations for the viscous flow, as developed in Sec. 7.20, suggest that $v_\theta = \tilde{v}_\theta \sin\theta$, so that Eq. 4, with cos θ factored out, becomes

$$\frac{2\sigma_o \tilde{v}_\theta}{R} = \sigma_b \tilde{E}_r^b = \sigma_b \left[-\frac{\tilde{\Phi}^b}{R} + \frac{3Id}{4\pi\sigma_b R^3} \right] \tag{5}$$

Here, Eq. 3 establishes the second equality.

The combination of electric double-layer boundary conditions, Eqs. 2.10.10 and 2.10.11, reduces here to

$$E_\theta = -\frac{1}{R}\frac{\partial \Phi^b}{\partial \theta} \tag{6}$$

serving as a reminder that just inside the interface there is a tangential electric field.

Stress Balance: The radial and tangential balance of mechanical stresses, with the surface force density given by Eq. 10.11.1 and with the shear term expressed as Eq. 10.11.14, are represented by

$$-\Pi^a + S_{rr}^a + \Pi^b - S_{rr}^b - \frac{2\gamma_e}{R} = 0 \tag{7}$$

$$S_{\theta r}^a - S_{\theta r}^b + \sigma_d E_\theta = 0 \tag{8}$$

With the outside potential defined as zero, it is appropriate to let Φ be the departure from potential V_d in the interior. Then

$$\gamma_e \approx \gamma_c - \sigma_d \Phi; \quad \sigma_d \equiv -\left(\frac{\partial \gamma_e}{\partial v_d}\right)_{V_d} \tag{9}$$

where γ_c is the surface tension at the equator and σ_d is in accordance with the Lippman Eq. 10.11.7. The θ-independent part of the surface tension radial force is balanced by a uniform pressure jump $\Pi^a - \Pi^b$ at the interface. With the assumption that $\sigma_d \approx \sigma_o$, Eq. 7 is satisfied for each value of θ if

$$2\tilde{S}_{rr}^a - 2\tilde{S}_{rr}^b + \frac{2\sigma_b}{R}\tilde{\Phi}^b = 0 \tag{10}$$

where cos θ has been factored out and amplitudes are introduced consistent with Table 7.20.1.

Similarly, according to Eqs. 8 and 6, tangential force equilibrium results at each value of θ if

$$\tilde{S}_{\theta r}^a - \tilde{S}_{\theta r}^b + \frac{\sigma_o}{R}\tilde{\Phi}^b = 0 \tag{11}$$

where sin θ is factored out.

That the double layer moves as a whole at a given interfacial location implies a tangential velocity at the interface that is continuous, while the assumption that spherical geometry is retained requires that the interior and exterior radial velocities vanish:

$$\tilde{v}_\theta^a = \tilde{v}_\theta^b; \quad \tilde{v}_r^a = 0; \quad \tilde{v}_r^b = 0 \tag{12}$$

With velocity amplitudes so related, viscous stresses are given for the outside region by Eq. 7.20.24 with the radius $\beta \to R$ and for the interior by Eq. 7.20.23 with radius $\alpha \to R$. These are now substituted into Eqs. 10 and 11. Three conditions on the amplitudes, physically representing conservation of charge, Eq. 5, and these radial and tangential interfacial stress balances are

$$\begin{bmatrix} \frac{2\sigma_o}{R} & \frac{\sigma_b}{R} & 0 \\ -\frac{3}{R}(\eta_a+2\eta_b) & \frac{2\sigma_o}{R} & \frac{3\eta_a}{2R} \\ -\frac{3}{R}(\eta_a+\eta_b) & \frac{\sigma_o}{R} & -\frac{3\eta_a}{2R} \end{bmatrix} \begin{bmatrix} \tilde{v}_\theta^b \\ \tilde{\Phi}^\beta \\ U \end{bmatrix} = \begin{bmatrix} \frac{3Id}{4\pi R^3} \\ 0 \\ 0 \end{bmatrix} \tag{13}$$

The velocity of the drop relative to an exterior fluid at infinity is the negative of U, where from Eq. 13

$$U = \frac{-Id}{4\pi R^2\sqrt{\sigma_b(\eta_a+\frac{3}{2}\eta_b)}} \frac{H_e}{(1+H_e^2)}; \quad H_e \equiv \frac{\sigma_o}{\sqrt{\sigma_b(\eta_a+\frac{3}{2}\eta_b)}} \tag{14}$$

The associated interfacial velocity follows by subtracting twice Eq. 13c from Eq. 13b,

$$\tilde{v}_\theta = -\frac{3U}{2} \tag{15}$$

With I and σ_o positive, the signs are consistent with Fig. 10.12.1 and the introductory discussion.

The normalized double layer charge density, H_e, also takes the form of an electric Hartmann number, $\sqrt{\tau_e/\tau_{EV}}$. This is seen by recognizing that $\sigma_o \to \varepsilon\mathscr{E}$ where $\mathscr{E}$ is typical of the electric field inside the layer. The dependence of U on H_e sketched in Fig. 10.12.3 makes it clear that an optimum charge density exists. With H_e small, the motion is mainly limited by viscosity and so increases in linear proportion to σ_o. But if $H_e >> 1$, then the interfacial velocity, and hence U, is limited by the ability of the electrolyte to conduct away the convected charge.

To discover what limits the magnitude of U, suppose that σ_o is made the optimum value so that $H_e = 1$. Then, Eq. 14 becomes

$$U_{opt} = \frac{-Id}{8\pi R^2\sigma_b}\sqrt{\frac{\sigma_b}{(\eta_a+\frac{3}{2}\eta_b)}} \tag{16}$$

The magnitude of I is limited by the maximum excursion of the double-layer potential from V_d. From Eqs. 13a and 15, the interfacial potential variation has the amplitude

$$\tilde{\Phi}^b = \frac{3Id}{4\pi R^2\sigma_b} + \frac{3\sigma_o}{\sigma_b}U \tag{17}$$

These voltage contributions are respectively due to conduction and convection. With $H_e = 1$, the second term cancels half of the first, so that the pole-to-pole excursion in potential, $2\tilde{\Phi}^b$, can be used to write Eq. 16 as

$$U_{opt} \to \frac{2\tilde{\Phi}^b}{6}\sqrt{\frac{\sigma_b}{(\eta_a+\frac{3}{2}\eta_b)}} \tag{18}$$

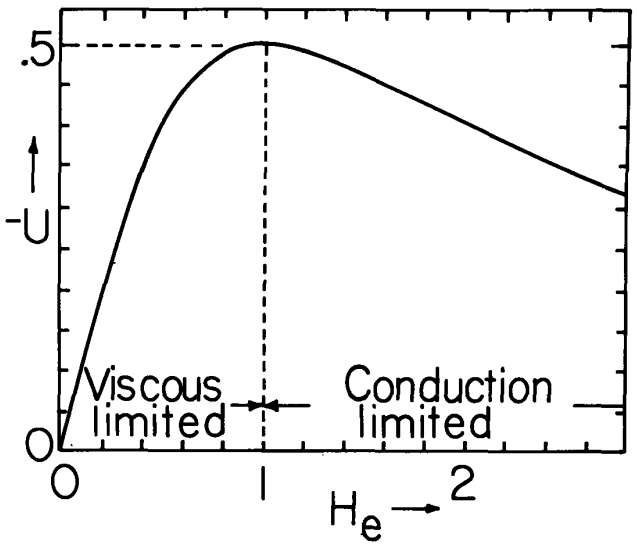

Fig. 10.12.3. Dependence of drop velocity on normalized double layer charge.

Typical values are $2\tilde{\Phi}^b = 0.1$ V, $\sigma_b = 10^{-2}$ mhos/m, $\eta_a = \eta_b = 10^{-3}$ for water based electrolytes, and hence velocities on the order of 3 cm/sec. Of course, the low Reynolds number condition may not be met with such a velocity. But clearly, the double layer mechanism can be the basis for significant motions.

The mechanical response to an electrical drive has been emphasized. That fields are generated by the motion is a reminder that the electrocapillary double layer can be the site of a reverse transduction.